

# Identifiable and interpretable nonparametric factor analysis

Maoran Xu

Department of Statistical Science, Duke University

Amy H. Herring

Department of Statistical Science, Global Health,  
and Biostatistics & Bioinformatics, Duke University

and

David B. Dunson

Departments of Statistical Science and Mathematics, Duke University

November 15, 2023

## Abstract

Factor models have been widely used to summarize the variability of high-dimensional data through a set of factors with much lower dimensionality. Gaussian linear factor models have been particularly popular due to their interpretability and ease of computation. However, in practice, data often violate the multivariate Gaussian assumption. To characterize higher-order dependence and nonlinearity, models that include factors as predictors in flexible multivariate regression are popular, with GP-LVMs using Gaussian process (GP) priors for the regression function and VAEs using deep neural networks. Unfortunately, such approaches lack identifiability and interpretability and tend to produce brittle and non-reproducible results. To address these problems by simplifying the nonparametric factor model while maintaining flexibility, we propose the NIFTY framework, which parsimoniously transforms uniform latent variables using one-dimensional nonlinear mappings and then applies a linear generative model. The induced multivariate distribution falls into a flexible class while maintaining simple computation and interpretation. We prove that this model is identifiable and empirically study NIFTY using simulated data, observing good performance in density estimation and data visualization. We then apply NIFTY to bird song data in an environmental monitoring application.

*Keywords:* Bayesian; Curse of dimensionality; Density estimation; Dimension reduction; Identifiability; Latent variables.

# 1 Introduction

Factor analysis (Fruchter, 1954; Harman, 1976) is a fundamental tool in various disciplines, including psychology, sociology, and medical research, where data often exhibit high dimensionality and strong dependence across features. Factor models learn a set of low-dimensional factors summarizing the high-dimensional data, which is useful in exploratory data analysis and in conducting inference on dependence structure. Given the observed data  $\mathbf{x}_1, \dots, \mathbf{x}_N \in \mathbb{R}^P$ , a factor model takes factors as predictors via a multivariate regression model, having the general form

$$\mathbf{x}_i = \mathbf{g}(\boldsymbol{\eta}_i) + \boldsymbol{\varepsilon}_i, \quad i = 1, \dots, N, \quad (1)$$

where  $\boldsymbol{\eta}_i \in \mathbb{R}^H$  denotes the low-dimensional latent factors with  $H \leq P$ ,  $\mathbf{g} : \mathbb{R}^H \rightarrow \mathbb{R}^P$  represents a mapping from the latent space to the data space and  $\boldsymbol{\varepsilon}_i$  denotes a  $P$ -dimensional residual.

A classical special case of (1) is the Gaussian linear factor model, which lets

$$\mathbf{x}_i = \boldsymbol{\Lambda}\boldsymbol{\eta}_i + \boldsymbol{\varepsilon}_i, \quad \boldsymbol{\eta}_i \sim N_H(\mathbf{0}, \mathbf{I}_H), \quad \boldsymbol{\varepsilon}_i \sim N_P(\mathbf{0}, \boldsymbol{\Sigma}), \quad i = 1, \dots, N, \quad (2)$$

where data  $\mathbf{x}_i$  are centered prior to analysis so that  $E(\mathbf{x}_i) = 0$  is a reasonable assumption. Here,  $\boldsymbol{\Lambda}$  is a  $P \times H$  factor loadings matrix, and the residual covariance matrix  $\boldsymbol{\Sigma}$  is typically assumed to be diagonal. Then, after marginalizing out the latent factors, a low rank plus diagonal factorization is induced for the covariance with  $\mathbf{x}_i \sim N_P(0, \boldsymbol{\Lambda}\boldsymbol{\Lambda}' + \boldsymbol{\Sigma})$ . There is a rich literature developing methods for inference under (2). Particularly relevant to this article is the Bayesian literature in which there has been abundant focus on careful choice of priors (Lopes and West, 2004; Carvalho et al., 2008), including to infer the number of factors (Bhattacharya and Dunson, 2011; Legramanti et al., 2020), efficient posterior computation (Ghosh and Dunson, 2009; Merkle and Rosseel, 2015), and interpretable inference on the factors via post-processing (Poworoznek et al., 2021; Papastamoulis and Ntzoufras, 2022).



Figure 1: Gaussian linear factor models for data violating normality. Left column: joint and marginals of 2D synthetic data. Middle column: joint and marginals of 2 latent factors. Right column: joint and marginals of data generated from the Gaussian linear factor model. Top row: Data points of 2 independent dimensions, one being right-skewed and the other bimodal. Bottom row: 2D data with Gaussian marginals but non-Gaussian dependence (dependence modeled by Clayton copula). In both examples,  $N = 400$ .

While the linear Gaussian form is convenient computationally and leads to simple interpretability, a concern is robustness to violations of normality. This motivated the copula factor model of Murray et al. (2013), which allows flexible marginal distributions but uses a Gaussian copula for the covariance; after transforming each of the features to be normally distributed, the resulting model is as in (2). However, it is common for features to have complex nonlinear relationships. Figure 1 shows how model (2) fails to capture non-Gaussian marginal distributions and nonlinear dependence across dimensions. When fitting a Gaussian latent factor model to these data, we find a problem of “distributional shift” in the fitted latent factors, see the mid-column in Figure 1—the distribution of the estimated factors  $\boldsymbol{\eta}_i$ , for  $i = 1, \dots, N$ , violates the normality assumption of the model. This leads to misleading interpretation of the model parameters and an inaccurate predictive distribution.

Limitations of linear factor models have been well-known for half a century (Gibson, 1960;

McDonald, 1962), motivating flexible nonlinear extensions. Classical approaches include parametric nonlinear terms (e.g., polynomial, exponential, interactions) in the factors (Yalcin and Amemiya, 2001; Arminger and Muthén, 1998). However, these approaches rely on pre-specified nonlinear functions. Alternatively, mixtures of factor analyzers use separate Gaussian linear factor models in different mixture components (Ghahramani et al., 1996; McLachlan et al., 2003). However, these models are heavily parameterized and can be brittle, especially when data exhibit nonlinearity but not distinct clusters. Alternatively, under a linear factor structure, the latent factors can be modeled nonparametrically. For example, using splines (Song and Lu, 2012) to estimate the relationship between outcome latent variables and explanatory latent variables, using additive basis functions (Sardy and Victoria-Feser, 2012; Bodelet and Shan, 2020) to improve flexibility, or mixtures of Gaussians (Chandra et al., 2023; Montanari and Viroli, 2010) for clustering of high-dimensional data. Modeling the distribution of the latent factors as nonparametric is related to the approach proposed in this paper. However, motivated by our focus on identifiability and interpretability, we develop novel models and theories.

In recent years, there has been abundant interest in probabilistic generative models, which seek to generate synthetic data that closely resemble training samples. Nonlinear factor models represent one broad class of probabilistic generative models, within a rich literature including normalizing flows (see Kobzyev et al. (2020) for a review) and generative adversarial networks (GANs, see Creswell et al. (2018) for a review). A potential advantage of nonlinear factor models is the ability to learn and exploit lower-dimensional structures in the data. However, in order to realize these advantages, and not simply provide a black box for synthetic data generation, it is important for the model to be identifiable. This is a prerequisite for reliable and reproducible dimensionality reduction and inferences.

Perhaps the two most popular approaches for flexible nonlinear factor analysis are variational auto-encoders (VAEs) (Kingma and Welling, 2014; Rezende et al., 2014) and Gaussian process latent variable models (GP-LVMs) (Li and Chen, 2016; Titsias and Lawrence, 2010). VAEs

use deep neural networks, and GP-LVMs use Gaussian processes to parameterize the mapping  $\mathbf{g}$  in (1). These methods are highly flexible and have succeeded in generating new data that closely resemble the training data. However, 1) the mappings and factors lack identifiability, with infinitely many solutions yielding the same likelihood; 2)  $\mathbf{g}$  is hard to interpret directly; 3) the function  $\mathbf{g}$  is a mapping from  $\mathbb{R}^H \rightarrow \mathbb{R}^P$ , so due to the curse of dimensionality, huge sample sizes may be needed; and 4) we have observed distributional shift between the empirical distribution of the estimated factors and the assumed distribution, badly degrading performance.

Inspired by the above, we fill the gap between simple but inflexible linear factor models and heavily parametrized nonidentifiable nonlinear factor models through our proposed nonparametric linear factor analysis (NIFTY) framework. With the same linear model as in (2), we let each  $\eta_{ih} \sim F_h$ . Instead of standard Gaussian-distributed factors, each factor can have any univariate continuous distribution. We model  $F_h$  nonparametrically by letting  $\eta_{ih} = g_h(u_{ih})$ , with  $u_{ih}$  uniformly distributed and  $g_h$  a transformation function characterized with monotonely non-decreasing linear splines. Therefore,  $g_h$  can be interpreted as the inverse cumulative distribution function (CDF) of  $F_h$ . A key innovation is to allow some of the  $u_{ih}$  to be identical, leading to dependence across the factors. We will show that our proposed models can accommodate rich nonlinear structures in the data. In addition, we show strict identifiability under mild assumptions, with the model structure enabling marginalization strategies to accelerate the mixing of a hybrid Langevin and Gibbs sampling algorithm. We empirically study the proposed NIFTY framework with simulated data and with an application to acoustic ecological monitoring data. NIFTY recovers meaningful latent factors and provides accurate uncertainty quantification across a variety of settings.

The rest of this paper is organized as follows. Section 2 introduces the model specification for NIFTY, along with a solution to the distributional shift problem. Section 3 contains identifiability results for the parameters in NIFTY, followed by Section 4 describing a technique to nail down the assumptions in Section 3. Section 5 displays simulated experiments and results,

comparing them to related methods. Section 6 applies the method to a bird song classification problem. Finally, Section 7 discusses implications and future directions.

## 2 The NIFTY Framework

### 2.1 Model specification

Suppose  $\mathbf{x}_1, \dots, \mathbf{x}_N \in \mathbb{R}^P$  are drawn from an unknown  $P$ -dimensional density  $f \in \mathcal{F}$ , with  $\mathcal{F}$  the set of densities with respect to Lebesgue measure on  $\mathbb{R}^P$ . We model this multivariate density via the following factor model:

$$\begin{aligned} \mathbf{x}_i &= \mathbf{\Lambda} \boldsymbol{\eta}_i + \boldsymbol{\varepsilon}_i, \quad \boldsymbol{\varepsilon}_i \sim N_P(\mathbf{0}, \boldsymbol{\Sigma}), \quad i = 1, \dots, N, \\ \eta_{ih} &= g_h(u_{ik_h}), \quad h = 1, \dots, H, \\ u_{ik} &\stackrel{\text{iid}}{\sim} U(0, 1), \quad k = 1, \dots, K, \quad K \leq H. \end{aligned} \tag{3}$$

Each latent factor  $\eta_{ih}$  is a transformation of a *latent location*  $u_{ik_h}$  via a *latent mapping*  $g_h$  which is a non-decreasing  $[0, 1] \rightarrow \mathbb{R}$  function. The subscript  $k_h$  creates a surjective mapping from  $\{1, \dots, H\}$  to  $\{1, \dots, K\}$ . By applying  $g_h := F_h^{-1}$  to a uniform variable, one gets  $\eta_{ih}$  with marginal CDF  $F_h$ . Throughout the paper we will assume a diagonal residual covariance  $\boldsymbol{\Sigma} = \text{diag}(\sigma_1^2, \dots, \sigma_P^2)$ . For simplicity of computation, we use monotone piecewise linear functions to model the 1-dimensional mappings.

The above generative model automatically induces a multivariate density  $\mathbf{x}_i \sim f$  while maintaining the simple interpretability of a linear latent factor model. Slightly abusing notation, let  $\mathbf{g}$  denote the vector-valued function  $(g_1, \dots, g_H)$  and  $\mathbf{g}(\mathbf{u}_i)$  denote the vector  $[g_1(u_{ik_1}), \dots, g_H(u_{ik_H})]$ . The density  $f$  is a deterministic function of  $\mathbf{\Lambda}, \mathbf{g}, \boldsymbol{\Sigma}$ , after marginalizing out the latent variable  $\mathbf{u}_i$  as

$$f_{\mathbf{\Lambda}, \mathbf{g}, \boldsymbol{\Sigma}} := f(\mathbf{x}_i; \mathbf{\Lambda}, \mathbf{g}, \boldsymbol{\Sigma}) = \int_{[0,1]^H} \phi_{\boldsymbol{\Sigma}}[\mathbf{x}_i - \mathbf{\Lambda} \mathbf{g}(\mathbf{u}_i)] d\mathbf{u}_i,$$

where  $\phi_{\Sigma}(\mathbf{x})$  refers to the density of a multivariate Gaussian with mean zero and covariance matrix  $\Sigma$  evaluated at  $\mathbf{x}$ . By assigning priors (to be specified in later sections)  $\Lambda \sim \Pi_{\Lambda}, g_h \sim \Pi_{g_h}, \Sigma \sim \Pi_{\Sigma}$ , we induce a prior for  $f$  with  $f \sim \Pi_f$ . We refer to  $f_{\Lambda, g, \Sigma}$  as the NIFTY model, and the induced prior for  $f$  as the NIFTY prior.

## 2.2 A Bayesian extension to ICA models

We now show that, in a special case, NIFTY reduces to an interesting type of Bayesian independent component analysis. The ICA model (Comon, 1994) assumes  $\mathbf{x}_i = \Lambda \boldsymbol{\eta}_i + \boldsymbol{\epsilon}_i$  with  $\eta_{ih}$  mutually independent and non-Gaussian. This model has been widely used in signal processing, for separating a compound, multivariate signal into additive, independent subcomponents. By choosing  $K = H$  in the NIFTY model, the mapping from uniform latent locations to latent factors is uniquely determined as  $k_h = h$ . Since  $u_{ik}$ s are iid,  $\eta_{ih}$ 's are mutually independent. With such a model, we are able to quantify multivariate distribution concentrated near a low-dimensional hyper-plane, with each factor following an arbitrary distribution. The following example illustrates the use of independent factors to characterize non-Gaussian multivariate distributions.

**Example 1.** (independent non-Gaussian distributions.) Suppose a 2-dimensional random vector  $\mathbf{x}_i$  consists of two independent entries  $x_{i1} \sim \text{Beta}(0.4, 0.4)$  and  $x_{i2} \sim \text{Gamma}(1, 1)$ . Figure 1 shows that the Gaussian linear factor model does not accommodate skewness and bimodality in the marginal distributions. In contrast, NIFTY (depicted in Figure 2) recovers the two non-Gaussian factors as transformations of two independent uniform latent variables.

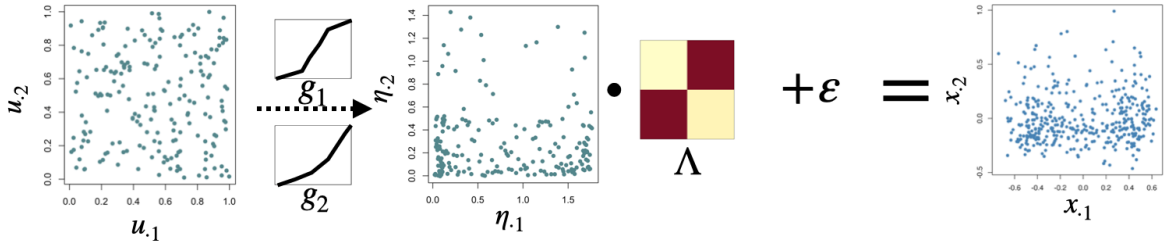


Figure 2: Illustration of NIFTY in the ICA special case. For data in example 1, NIFTY learns two mutually independent uniform variables  $u_1$  and  $u_2$ , mapped to  $\eta_1$  and  $\eta_2$  via  $g_1$  and  $g_2$ .

ICA models are unable to characterize nonlinear dependence among the dimensions. For example, when  $x_{i1} = p(x_{i2})$  with  $p(\cdot)$  a polynomial function, ICA performs poorly in inferring the components. We solve this limitation by a novel model construction: by allowing  $\eta_{ih}$ 's mapped from the same uniform location  $u_{ik_h}$ , we introduce dependence among the factors. If  $k_{h_1} = k_{h_2}$ , then  $\eta_{ih_1}$  is a nonlinear transformation from  $\eta_{ih_2}$ , otherwise  $\eta_{ih_1}$  and  $\eta_{ih_2}$  are independent. Thus, we broaden the class of densities characterized by an ICA model to accommodate wider nonlinear dependence. We illustrate in Figure 3 the difference between the general NIFTY model and the special case of Bayesian ICA.

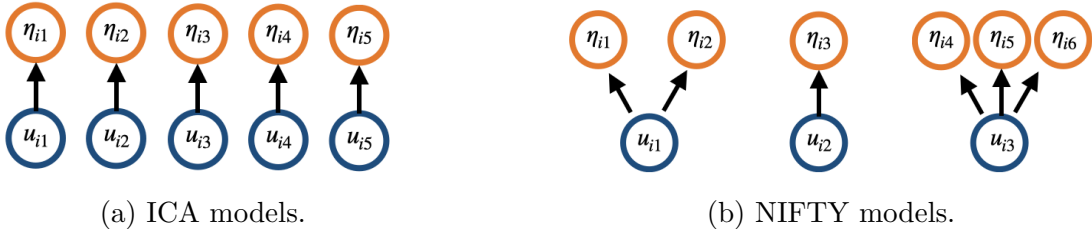


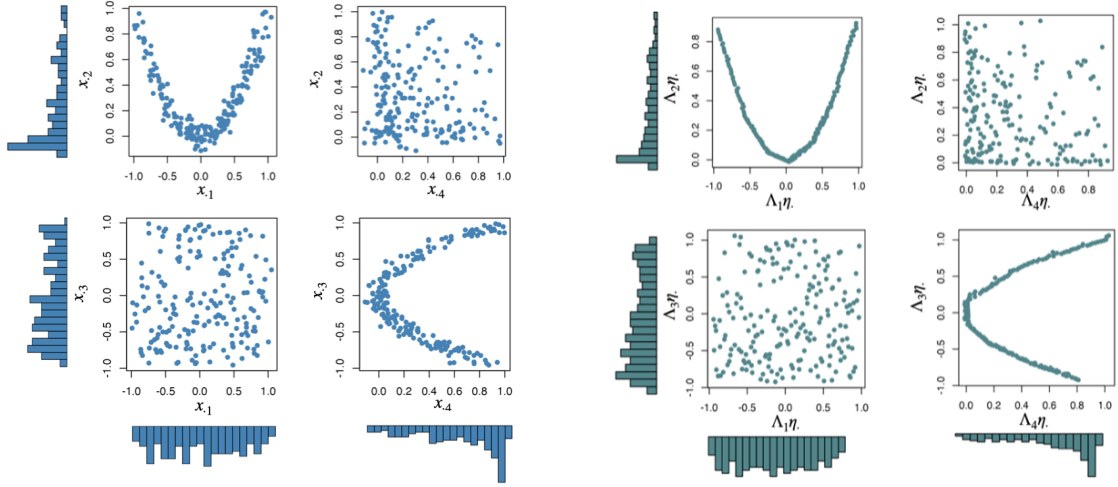
Figure 3: Illustrating the 1-dimensional mapping procedure from uniform latent locations to latent factors in (a) special case of ICA model and (b) general NIFTY models.

The following example illustrates the flexibility that can be achieved by a NIFTY model with both independent and dependent factors; in this case, the latent structure consists of two independent curves.

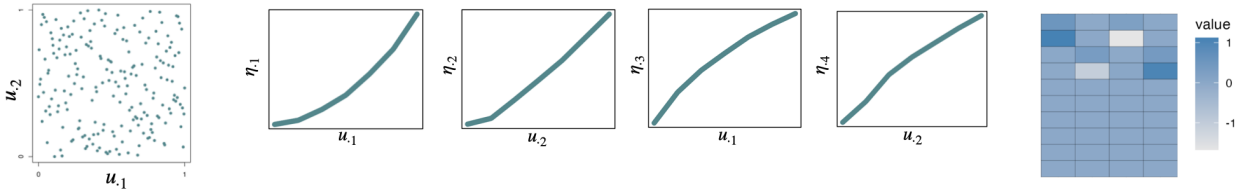
**Example 2.** (Two curves.) We generate data  $\mathbf{x}_i$  from  $N_{10}[(2z_{i1}, 2z_{i1}^2, 2z_{i2}, 2z_{i2}^2, 0, \dots, 0), \sigma^2 \mathbf{I}_{10}]$  with  $\sigma^2 = 0.01$  and  $z_{ij} \stackrel{\text{iid}}{\sim} \text{Beta}(0.5, 0.5)$  for  $j = 1, 2$ . The pairwise plot and marginal histograms are shown in Figure 4(a). NIFTY learns the generative process from two independent uniform



variables  $u_1$  and  $u_2$  mapped to  $\eta_1, \dots, \eta_4$  via  $g_1, \dots, g_4$ , and linearly mapped to the data space. We postpone the details of this numerical experiment along with a comparison with other methods in Section 5.



(a) The first four dimensions of  $\mathbf{x}_i$  generated from two latent curves. (b) The fitted components  $\Lambda\eta_i$  generated from two latent curves.



(c) Uniform latent locations.

(d) Latent mappings  $g_1, g_2, g_3$  and  $g_4$ .

(e) Loading matrix.

Figure 4: An illustration of the NIFTY+ framework on 10-dimensional data arising from two latent curves. Starting from the independent latent locations (c), the framework learns four mappings (d) and transforms the uniform latent variables to latent factors  $\eta_1, \dots, \eta_4$ , along with a loading matrix (e). The fitted components accurately infer the two independent latent curves.

### 2.3 Solving distributional shift: uniform constraint

As noted in Section 1, latent factor models often face a problem of posterior distributional shift, which is typically ignored in the current literature. In this subsection, we first describe distributional shift and then propose a constraint relaxation approach (following the notion by Duan et al. (2020)) to solve this problem in NIFTY.

Consider the general factor model in (1). In most settings, the density of the latent factors  $\eta_i$  is fixed in advance, say as  $F_0$ . For example, it is common to let  $\eta_i \sim F_0 \equiv N_H(\mathbf{0}, \mathbf{I}_H)$ . Then,

taking a Bayesian approach, one infers the posterior distribution for the latent factors  $\{\boldsymbol{\eta}_i\}$  and the parameters characterizing  $\boldsymbol{g}(\cdot)$  and the distribution of the residuals. Subsequent inferences and predictions are based on the assumption that the population distribution of the latent factors is exactly  $F_0$ . However, in practice, it is common for the empirical distribution of the inferred latent factors to deviate substantially from  $F_0$ . The inferred population parameters compensate for this deviation to produce a good in-sample fit but with a potentially devastating impact on parameter inferences and out-of-sample predictions.

To provide a simple motivating example, consider the Gaussian linear factor model in (2). Suppose that distributional shift occurs, so that the empirical distribution of  $\{\boldsymbol{\eta}_i\}$  is far from standard normal *a posteriori* with significant deviations from identity covariance. Then, in order to provide a good fit to the data, the posterior on  $\boldsymbol{\Lambda}$  and  $\boldsymbol{\Sigma}$  will compensate so that the empirical covariance of  $\boldsymbol{x}_i, i = 1, \dots, N$ , is close to  $\boldsymbol{\Lambda}\text{cov}(\boldsymbol{\eta}_i, i = 1, \dots, N)\boldsymbol{\Lambda}^T + \boldsymbol{\Sigma}$ . This compensation can lead to considerable bias in the usual factor analysis covariance estimator of  $\boldsymbol{\Lambda}\boldsymbol{\Lambda}^T + \boldsymbol{\Sigma}$ . We provide an example of such bias in the Supplementary Materials.

The distributional shift also occurs for flexible nonlinear factor models. For example, Variational Auto-Encoders (VAEs) use deep neural networks for  $\boldsymbol{g}(\cdot)$ . This leads to a non-identifiability problem between the latent factors and  $\boldsymbol{g}(\cdot)$ . As long as the mapping can project the learned factors near the data to minimize the target loss function, the factors can take any distribution *a posteriori*. Indeed, we provide examples in the Supplementary Materials showing substantial deviation between the empirical distribution of the inferred factors *a posteriori* and their *a priori* assumed distribution. This is different from the well-known “posterior collapse” behavior of VAEs in which there is a lack of learning from the data about the latent variables (Dai et al., 2020; Wang et al., 2021).

As a remedy to posterior drift, we propose to constrain the empirical distribution of the latent factors to be close to  $F_0$  *a posteriori*. For NIFTY this equates to restricting the distribution of

the  $u_{ik}$ s to be very close to uniform. To accomplish this, for each  $k = 1, \dots, K$ , we let

$$\Pi_{\mathbf{u}_k}(u_{1k}, \dots, u_{Nk}) = \prod_{i=1}^N 1(u_{ik} \in [0, 1]) \exp(-\nu \mathcal{W}_2(U_k, U)), \quad (4)$$

where  $\mathcal{W}_2(U_k, U)$  denotes the Wasserstein-2 distance between the empirical distribution of  $u_k$  and a  $U(0, 1)$  variable. The exponential term introduces a continuous relaxation of the uniform distributional constraint, with hyper-parameter  $\nu > 0$  controlling distance from uniform. The Wasserstein distance measures the optimal transport distance (Kolouri et al., 2017) between two distributions. The Wasserstein-2 distance between univariate random variables with CDFs  $F$  and  $G$  is  $\mathcal{W}_2(F, G) = \left( \int_0^1 |F^{-1}(z) - G^{-1}(z)|^p dz \right)^{1/p}$ . As an approximation of  $\mathcal{W}_2(U_k, U)$ , let

$$\hat{\mathcal{W}}_2(U_k, U) = \left( \sum_{i=1}^N \|u_{(i)k} - u_{(i)}^0\|^2 \right)^{1/2},$$

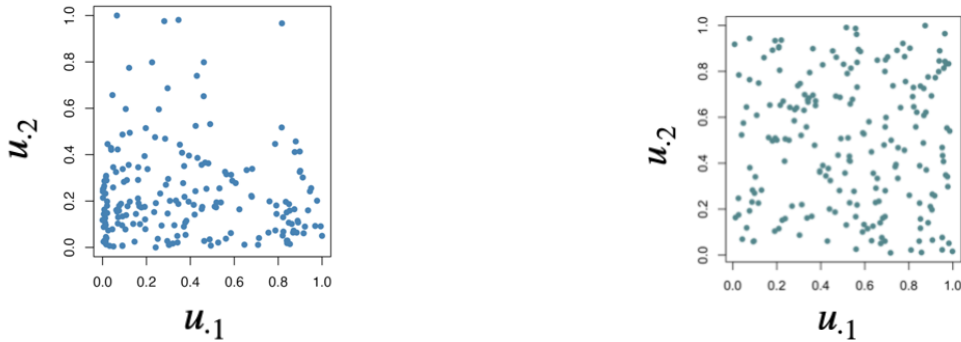
where  $u_{(i)k}$  is the  $i$ th order statistic of  $\{u_{1k}, \dots, u_{Nk}\}$  and  $u_{(i)}^0 = i/N$ .

**Proposition 1.** *Suppose  $u_{1k}, \dots, u_{Nk}$  are assigned prior (4). Then the prior distribution of  $u_{ik}$  converges in distribution to  $U(0, 1)$ , as  $\nu \rightarrow \infty$  and  $N \rightarrow \infty$ .*

Refer to the appendix for proof of the proposition and the Supplementary Materials for a simulation experiment shedding light on how to choose the key hyperparameter  $\nu$  in practice. Through empirical analysis, we find that  $\nu$  yields the best results when it lies within the range of  $10^2$  and  $10^3$ . In general,  $\nu$  needs to be large enough to strongly constrain the empirical distribution but huge values can lead to slow mixing. The following example provides an illustration.

**Example 1** (Continued). Continuing the example of non-Gaussian marginals, we compare NIFTY with and without the (soft) prior constraint. From panel (a) in Figure 5, without the constraint, the distribution of the latent  $(u_{i1}, u_{i2})$ s deviates from the 2-dimensional independent uniform distribution, and shifts towards the data distribution. As a result, the nonlinear mappings  $g_1$  and  $g_2$  are nearly identity maps. Adding the distributional constraint in the prior

enables us to reliably fit and interpret the nonparametric factors.



(a) One posterior sample of the latent locations without the constraint relaxation term.

(b) One posterior sample of the latent locations with the constraint relaxation term ( $\nu = 1000$ ).

Figure 5: Comparing NIFTY results with and without the (soft) prior distributional constraint in example 1. Without the constraint, the latent locations deviate from the 2-dimensional independent uniform distribution, and shift towards the data distribution.

### 3 Identifiability Results

Identifiability is a key property for a latent variable model to provide reliable, reproducible, and interpretable latent representations. There are two notions of identifiability for factor models (introduced by Allman et al. (2009)), *strict identifiability* and *generic identifiability*. Strict identifiability ensures the mapping from the observed data to the parameters is one-to-one, and generic identifiability only requires the mapping be one-to-one except on a Lebesgue measure zero subset of the parameter space.

In this section, we establish strict identifiability for  $\Lambda$ ,  $\Sigma$  and the parameterization of  $g_1, \dots, g_h$  in two steps. First, under a mild anchor dimension assumption, we show the parameters and factors are unique up to a simple transformation, leading to generic identifiability. Second, based on the ambiguity set of parameters yielding an equivalent likelihood, we propose simple post-processing steps to remove ambiguity. This leads to strict identifiability, which in turns allows us to show posterior consistency.

We start with formal definitions of the two notions of identifiability.

**Definition 1.** (*Strict Identifiability*). Latent factor model (3) is strictly identifiable if

$$pr(\mathbf{x}_i = \mathbf{a} \mid \Lambda, \mathbf{g}, \mathbf{u}_i, \Sigma) = pr(\mathbf{x}_i = \mathbf{a} \mid \Lambda', \mathbf{g}', \mathbf{u}'_i, \Sigma') \quad \forall \mathbf{a} \in \mathbb{R}^P$$

holds if and only if  $(\Lambda, \mathbf{g}, \mathbf{u}_i, \Sigma)$  and  $(\Lambda', \mathbf{g}', \mathbf{u}'_i, \Sigma')$  are identical up to a latent class permutation.

**Definition 2.** (*Generic Identifiability*). Latent factor model (3) is generically identifiable if the set  $\mathcal{S}_{(\Lambda, \mathbf{g}, \Sigma)} := \{(\Lambda', \mathbf{g}', \Sigma') : pr(\mathbf{x}_i = \mathbf{a} \mid \Lambda, \mathbf{g}, \Sigma) = pr(\mathbf{x}_i = \mathbf{a} \mid \Lambda', \mathbf{g}', \Sigma'), \forall \mathbf{a} \in \mathbb{R}^P\}$  has Lebesgue measure zero.

### 3.1 Generic identifiability with anchor dimension assumption

In nonlinear latent factor models, the model parameters are usually nonidentifiable without additional assumptions or constraints (Yalcin and Amemiya, 2001). Our identifiability results build on related theory for factor models including Bing et al. (2020); Arora et al. (2013); Moran et al. (2022). These works assume the existence of “anchor features” (or “pure variables”), which refers to certain dimensions of data that depend on only one factor. For now, we similarly assume pre-specified anchor features, but we later introduce a pretraining approach to learn the anchor dimensions leveraging on diffusion maps (Coifman and Lafon, 2006). In our NIFTY framework, an anchor dimension is a dimension in the data that depends on only one latent location, with a formal definition as follows.

**Definition 3.** (*Anchor dimension*) A dimension  $j$  is said to be an anchor dimension for latent location  $u_{ik}$  if  $x_{ij}$  only depends on that variable. That is, there exists an index  $h$  with  $k_h = k$ , such that  $E(x_{ij} \mid \mathbf{u}_i) = \lambda_{jh} g_h(u_{ik})$  for all  $i$ . The  $x_{ij}$  is known as the anchor feature.

**Assumption 1.** (*Anchor feature*) For each factor  $u_{ik}$  in model (3), there exists at least one anchor feature.

It is trivial to notice that  $(\lambda_{jh}, g_h)$  can be equivalently expressed as  $(a\lambda_{jh}, \frac{1}{a}g_h)$  for any scalar

$a > 0$ . To avoid the trivial scaling ambiguity, we assume the columns of  $\mathbf{\Lambda}$  are scaled and the loading matrix is of full column rank.

**Assumption 2.** (*Scaled and full-ranked loadings*) *The loading matrix  $\mathbf{\Lambda}$  is of full column rank.*

*Letting  $\Lambda_h$  denote the  $h$ th column of  $\mathbf{\Lambda}$ , we have  $\|\Lambda_h\|_2 = 1$ .*

We let  $j_1, \dots, j_K$  denote the anchor dimensions of  $u_1, \dots, u_K$ . When the data and model satisfy Assumptions 1-2, we can express each anchor dimension in the data as

$$x_{ij_k} = \lambda_{j_k h} g_h(u_{ik}) + \varepsilon_{ij_k}, \quad \varepsilon_{ij_k} \sim N(0, \sigma_{ij_k}^2). \quad (5)$$

Without further constraints, it is also impossible to identify the diagonal covariance matrix for the residuals. For example, in a one-dimensional factor model,  $x_i = \eta_i + \varepsilon$  can be equivalently expressed by  $x_i = (\eta_i + \varepsilon/2) + \varepsilon/2$  with  $\gamma_i = (\eta_i + \varepsilon/2)$  interpreted as the latent factor. The following assumption avoids this ambiguity. While this assumption may seem overly restrictive, in the next section we develop a pretraining method to augment the observed data with inferred anchor features whose variances can be estimated and fixed in advance of analysis with our Bayesian nonparametric factor model.

**Assumption 3.** (*Residual variance of the anchor features*) *The residual variance of each anchor feature is known.*

We now state the generic identifiability of the NIFTY model. Recall the model setting in (3) and that the  $H$  factors are mapped from  $K$  uniform latent locations. We introduce a partition according to the mapped latent location: let  $\boldsymbol{\eta}_i^1, \dots, \boldsymbol{\eta}_i^K$  be a partition of  $\boldsymbol{\eta}_i$ , such that each  $\boldsymbol{\eta}_i^k$  consists of factors mapped from uniform location  $u_{ik}$ . Let  $\mathbf{\Lambda}^1, \dots, \mathbf{\Lambda}^K$  be the partition in the columns of  $\mathbf{\Lambda}$  and  $\mathbf{g}^1, \dots, \mathbf{g}^K$  be the partition of  $\mathbf{g}$ , according to the same logic.

**Theorem 1.** *Suppose the data and model (3) satisfy Assumptions 1-3, and the parameters are partitioned into groups according to the latent locations. Then we have*

- (generic identifiability of  $\Lambda$  and  $\mathbf{g}$ )

$$pr(\mathbf{x}_i = \mathbf{a} \mid \Lambda, \mathbf{g}) = pr(\mathbf{x}_i = \mathbf{a} \mid \Lambda', \mathbf{g}') \quad \forall \mathbf{a} \in \mathbb{R}^P$$

holds if and only if there exists rotation matrices  $\mathbf{R}^1, \dots, \mathbf{R}^K$  such that  $\mathbf{R}^k(\mathbf{R}^k)^T = \mathbf{1}$  and that  $\Lambda^k = \Lambda'^k \mathbf{R}^k$ , and  $\mathbf{g}^k(\mathbf{u}) = (\mathbf{R}^k)^T \mathbf{g}'^k(\mathbf{u})$  for all  $\mathbf{u}$ .

- (strict identifiability of the Gaussian noise) The covariance matrix  $\Sigma$  is unique.

### 3.2 Strict identifiability after post-processing

It is standard practice in the Bayesian factor analysis literature to apply post-processing to account for identifiability issues in inferring the factor loadings matrix in Gaussian linear factor models. We build on such approaches to develop a post-processing algorithm to infer parameters satisfying strict identifiability. After we obtain  $M$  posterior samples from MCMC as  $(\Lambda^{(1)}, \mathbf{g}^{(1)}, \Sigma^{(1)}), \dots, (\Lambda^{(M)}, \mathbf{g}^{(M)}, \Sigma^{(M)})$ , we apply the following steps.

---

**Algorithm 1: post-processing the posterior samples to solve ambiguity**

---

**Input:**  $(\Lambda^{(1)}, \mathbf{g}^{(1)}, \Sigma^{(1)}), \dots, (\Lambda^{(M)}, \mathbf{g}^{(M)}, \Sigma^{(M)})$

**for**  $m = 1, \dots, M$  **do**

**for**  $k = 1, \dots, K$  **do**

Orthogonalize the  $k$ th partition  $\Lambda^{(m)k}$  and tackle the label and sign switching with `MatchAlign` algorithm (Poworoznek et al., 2021);

Obtain rotation matrix  $\mathbf{R}^{(m)k}$  and  $\Lambda_h^{(m)k} \leftarrow \Lambda^{(m)k} \mathbf{R}^{(m)k}$ ;

Rotate  $\mathbf{g}^k$  and obtain  $\mathbf{g}^{(m)k} \leftarrow (\mathbf{R}^{(m)k})^T \mathbf{g}^{(m)k}$ .

**for**  $h = 1, \dots, H$  **do**

$\Lambda_h^{(m)} \leftarrow \Lambda_h^{(m)} / \|\Lambda_h^{(m)}\|_2$ ;

$\mathbf{g}^{(m)} \leftarrow \mathbf{g}^{(m)} \|\Lambda_h^{(m)}\|_2$ ;

---

After the post-processing, we have strict identifiability for each parameter.

**Proposition 2.** *Suppose the data and model (3) satisfy Assumptions 1-3. After the post-processing steps described in Algorithm 1, the model parameters  $(\mathbf{\Lambda}, \mathbf{g}, \mathbf{\Sigma})$  are strictly identifiable.*

### 3.3 Posterior consistency

With the identifiability results, we achieve guaranteed posterior consistency under suitable priors. We first show Bayesian posterior consistency for the model parameters, then develop a large support property for the induced density, in order to show the induced density also has posterior consistency in a strong sense.

**Theorem 2.** *(Posterior consistency of parameters) Denote the collection of model parameters by  $\Theta = (\mathbf{\Lambda}, \mathbf{g}, \mathbf{\Sigma})$ . Suppose the prior distribution for the parameters has full sup-norm support around the true value  $\Theta^0$  and the data satisfy Assumptions 1-3. Let  $H(\Theta)$  denote the post-processed parameters under Algorithm 1. Then for any  $\epsilon$ -neighborhood around  $\Theta^0$ ,  $\mathcal{N}_\epsilon(\Theta^0)$ ,*

$$pr(H(\Theta) \in \mathcal{N}_\epsilon(\Theta^0) \mid \mathbf{x}_1, \dots, \mathbf{x}_N) \rightarrow 1 \quad P_0^\infty \text{ almost surely.}$$

Next, we establish the posterior consistency of the induced density of  $\mathbf{x}_i$ . As a mild condition, the true density generating the data should be close to a latent factor structure described by model 3, which is formulated as follows.

**Assumption 4.** *There exists  $\mathbf{\Lambda}^0 \in \mathbb{R}^{P \times H}$ ,  $\mathbf{g}^0 = (g_1^0, \dots, g_h^0)$ , and  $\mathbf{\Sigma}^0 = \text{diag}\{(\sigma_1^0)^2, \dots, (\sigma_P^0)^2\}$  such that the  $P$ -dimensional multivariate density can be represented as*

$$f^0(\mathbf{x}_i) = \int_{[0,1]^H} \phi_{\mathbf{\Sigma}^0}[\mathbf{x}_i - \mathbf{\Lambda}^0 \mathbf{g}^0(\mathbf{u}_i)] d\mathbf{u}_i, \quad (6)$$

*with  $\sup |g_h^0(u)| < \infty$  for any  $u \in [0, 1]$ , and  $f^0$  strictly positive and finite.*

The next theorem states that the induced prior on the density  $f$  assigns positive probability to arbitrary small neighborhoods of any  $f_0$  satisfying Assumption 4. The neighborhoods are



defined using Kullback-Leibler (KL) divergence. For two continuous distributions with densities  $f_1$  and  $f_2$ , the KL divergence is defined to be

$$KL(f_1, f_2) = \int f_1(\mathbf{x}) \log \frac{f_1(\mathbf{x})}{f_2(\mathbf{x})} d\mathbf{x}.$$

We denote an  $\epsilon$ -sized KL neighborhood around a density  $f^0$  as  $KL_\epsilon(f^0)$ .

**Theorem 3.** *Suppose data are generated from model (3), with true parameter  $\Theta^0$ . Let  $f^0$  denote the corresponding density. Suppose the prior distribution has full sup-norm support around the true value  $\Theta^0$  and the data satisfy Assumption 1-3, then  $\Pi_f[KL_\epsilon(f^0)] > 0$  for all  $\epsilon > 0$ .*

Given the identifiability and large prior support results, we conclude this section with the consistency result of density estimation.

**Proposition 3.** *Suppose data are generated from model (3) and satisfy Assumption 1. Let  $f^0$  denote the corresponding density. If the priors for  $\Lambda, \mathbf{g}, \Sigma$  satisfy the conditions in Theorem 3, then the posterior distribution of the induced  $f$  converges as follows:*

$$\Pi[\mathcal{U}_\epsilon(f^0) \mid \mathbf{x}_1, \dots, \mathbf{x}_N] \rightarrow 1 \quad \mathbb{P}_0^\infty\text{-almost surely,}$$

where  $\mathcal{U}_\epsilon(f^0) := \{f : \int |f - f^0| d\mathbf{x} < \epsilon\}$  is an  $\epsilon$ -ball around the true density, and  $\mathbb{P}_0^N$  denotes the distribution of  $\mathbf{x}_1, \dots, \mathbf{x}_N$  under  $f^0$ .

Note that the conditions needed for posterior consistency of the parameters are more stringent than what is needed for posterior concentration of the induced density of the data around the truth. In particular, we can avoid Assumptions 2-3. While Assumption 2 is trivially satisfied with appropriate priors and post-processing, Assumption 3 is much more stringent. Indeed, in practice the values of the noise variance for the anchor features would not be known. We address this problem with appropriate pre-processing in the next Section.

## 4 Augmenting anchor data with diffusion maps

The anchor dimension assumption (1) seems restrictive since usually we do not have knowledge about how many latent factors there are or which dimensions can be treated as anchor dimensions. In this paper, we suggest *pretraining* steps to produce augmented anchor data.

In developing nonlinear factor models, a key motivation is accommodating data concentrated close to a lower-dimensional and potentially nonlinear subspace. This motivates pretraining based on diffusion maps (Coifman and Lafon, 2006), a popular nonlinear dimension reduction method. In later sections, we demonstrate the use of t-SNE (Van der Maaten and Hinton, 2008) as an alternative to diffusion maps.

The basic idea of diffusion-map-based pretraining is to automatically learn the intrinsic dimension  $K$  and compute a  $K$ -dimensional coordinate that preserves the local geometry in the original data. The pretraining can be summarized in the following steps:

1. Given the  $P$ -dimensional data  $\mathbf{x}_1, \dots, \mathbf{x}_N$ , use diffusion maps to learn a  $Q$ -dimensional representation, denoted by  $\mathbf{x}_i^* = (x_{i1}^*, \dots, x_{iQ}^*)$ . The diffusion map can be summarized as follows:

- Define a distance matrix in  $\mathbb{R}^P$  as

$$\kappa(\mathbf{x}, \mathbf{x}') = \exp\left(-\frac{\|\mathbf{x} - \mathbf{x}'\|_{\mathbb{R}^D}^2}{\epsilon_{DM}^2}\right),$$

where  $\epsilon_{DM}$  is a tuning parameter. In practice, we follow the criteria in Shan and Daubechies (2022) to tune  $\epsilon_{DM}$ .

- Let  $W_{ij} = \frac{\kappa(\mathbf{x}_i, \mathbf{x}_j)}{d(\mathbf{x}_i)d(\mathbf{x}_j)} \in \mathbb{R}^{N \times N}$ ,  $1 \leq i, j, \leq N$ , where  $d(\mathbf{x}_i) = \sum_{j=1}^N \kappa(\mathbf{x}_i, \mathbf{x}_j)$ .
- Define an  $N \times N$  diagonal matrix  $D$  as  $D_{ii} = \sum_{j=1}^N W_{ij}$ , where  $i = 1, \dots, N$ .
- Define the normalized graph Laplacian  $L$  as  $L = \frac{D^{-1}W - I}{\epsilon_{DM}^2} \in \mathbb{R}^{N \times N}$ .
- Let  $(\mu_j, \mathbf{v}_j)_{j=0}^{N-1}$  denote the eigenpairs of  $-L$  with  $\mu_0 \leq \mu_1 \leq \dots \leq \mu_{N-1}$  and  $\mathbf{v}_j$ 's are

unit  $N$ -vectors. Then  $\mu_0 = 0$  and  $\mathbf{v}_0$  is a constant vector. Take the first  $Q$  eigenvectors corresponding to the  $Q$  largest eigenvalues,  $(\mathbf{v}_1, \dots, \mathbf{v}_Q)$ , as coordinates for the data set  $\{\mathbf{x}_i\}_{i=1}^N$  in a  $Q$ -dimensional space.

2. Construct a *local covariance matrix* (proposed in Dunson and Wu (2021)) at each point  $\mathbf{x}_i^*$  using the coordinates learned in step 1, which is defined as

$$C_{N,\epsilon}(\mathbf{x}_i^*) = \frac{1}{N} \sum_{i'=1}^N (\mathbf{x}_i^* - \mathbf{x}_{i'}^*) (\mathbf{x}_i^* - \mathbf{x}_{i'}^*)^\top \mathbf{1}(\|\mathbf{x}_i^* - \mathbf{x}_{i'}^*\|_2 \leq \epsilon)$$

3. Define  $\lambda_{N,\epsilon,m}(\mathbf{x}_i^*)$  to be the  $m$ th largest eigenvalue in  $C_{N,\epsilon}(\mathbf{x}_i^*)$ . Then define the mean of the  $m$ th eigenvalues of the local covariance matrices as  $\bar{\lambda}_{\epsilon,m} = \frac{1}{N} \sum_{i=1}^N \lambda_{N,\epsilon,m}(\mathbf{x}_i^*)$ .
4. Determine the dimension to be  $K$  with respect to a threshold  $\delta$ :  $K = \max\{k : \bar{\lambda}_{\epsilon,k+1}/\bar{\lambda}_{\epsilon,k} \geq \delta\}$ . We take  $\delta = 0.5$  as a default choice.
5. After determining the dimension  $K$ , we take the first  $K$  dimensions  $(x_{i1}^*, \dots, x_{iK}^*)$  as the anchor data. We henceforth use  $\mathbf{x}^* \in \mathbb{R}^{N \times K}$  to denote the augmented anchor data.
6. Estimate the residual variances: for each  $k$ , let  $u_{ik}^* = r/N$  if  $x_{ik}^*$  is ranked the  $r$ th smallest among  $x_{1k}^*, \dots, x_{Nk}^*$ . Fit a piecewise-linear regression model  $x_{ik}^* = \alpha_0 + \sum_{l=1}^L \alpha_l (u_{ik}^* - \frac{l-1}{L}) \mathbf{1}_{\{u_{ik}^* \in [\frac{l-1}{L}, \frac{l}{L}]\}} + \epsilon_i$ ,  $\epsilon_i \sim N(0, \sigma_k^2)$  and denote the fitted value of the least square estimator as  $\hat{x}_{1k}^*, \dots, \hat{x}_{Nk}^*$ . Set  $\hat{\sigma}_k^2 = \frac{\sum_{i=1}^N (\hat{x}_{ik}^* - x_{ik}^*)^2}{N-L-2}$  as the residual variance for the  $k$ th anchor feature in Assumption 3.

Let  $M$  be a  $K$ -dimensional smooth, closed and connected Riemannian manifold isometrically embedded in  $\mathbb{R}^P$  through  $\iota : M \rightarrow \mathbb{R}^P$ . Coifman and Lafon (2006) show that the negative of the graph Laplacian approximates the Laplace-Beltrami operator of  $M$  pointwisely. By choosing an appropriate  $\epsilon_{DM}$  and bandwidth in the local covariance matrix, the augmented data approximates the discretization of an embedding of  $\iota(M)$  into  $\mathbb{R}^P$ . We numerically find this algorithm stable and

useful for extracting latent features. As shown in Figure 6, the diffusion-map-based pretraining produces two augmented anchor dimensions that recover the true latent variables generating the data in example 2.

## 5 Numerical Experiments

### 5.1 Density estimation and factor analysis

We first use three different simulated datasets to assess performance in density and parameter estimation. We then compare with Gaussian linear factor models, GP-LVMs, and variational auto-encoders in terms of density estimation accuracy and latent variable interpretability. We consider the following three simulation settings:

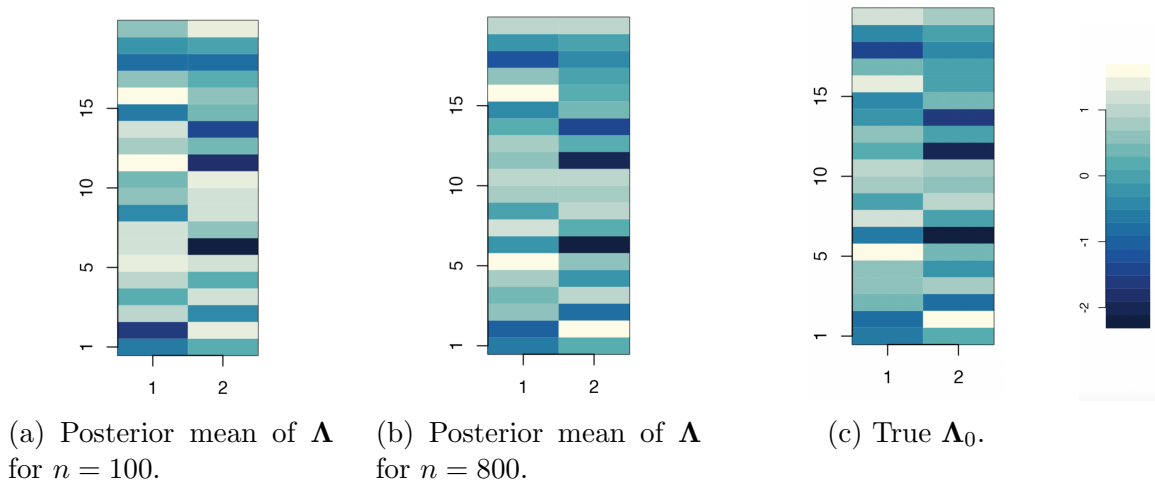
1. Independent but non-Gaussian marginal distribution in  $\mathbb{R}^2$ :  $\mathbf{x}_i = N[(z_{i1}, z_{i2})^T, \sigma^2 \mathbf{I}_2]$ ,  $z_{i1} \sim \text{Beta}(0.4, 0.4)$ ,  $z_{i2} \sim \text{Gamma}(1, 1)$ ,  $\sigma^2 = 0.01$ ,  $z_{i1} \perp\!\!\!\perp z_{i2}$ .
2. Gaussian linear factor in  $\mathbb{R}^{20}$ :  $\mathbf{x}_i = \mathbf{\Lambda}\boldsymbol{\eta}_i + \boldsymbol{\varepsilon}_i$ ,  $\boldsymbol{\eta}_i \sim N_2(0, \mathbf{I}_2)$ ,  $\sigma^2 = 0.01$ ,  $\lambda_{jk} \stackrel{\text{iid}}{\sim} N(0, 1)$ .
3. Curved shape in  $\mathbb{R}^{10}$ :  $\mathbf{x}_i = N[(2z_{i1}, 2z_{i1}^2, 2z_{i2}, 2z_{i2}^2, 0, \dots, 0)^T, \sigma^2 \mathbf{I}_{10}]$  with  $\sigma^2 = 0.01$  and  $z_{ij} \stackrel{\text{iid}}{\sim} U(0, 1)$ .

In each experiment, we generated  $n$  data points and varied the training size  $n$  from 100 to 800 to examine the impact of sample size on model performance. We use the diffusion-map-based algorithm to pretrain a set of anchor data for each case. For all three settings, the pretraining yields two anchor dimensions, which coincides with the true number of independent latent variables. Figure 6 displays a sanity check for the augmented data in setting 1. The anchor data recover the true independent factors that generate the dataset.



Figure 6: Anchor data of setting 1 learned from diffusion maps, plotted against true latent variables.

We analyze simulated data using a Metropolis-within-Gibbs sampler; the details are postponed to the Supplementary Materials. For each MCMC chain, we run 10,000 iterations, discarding the first 5,000 as a burn-in. We apply the post-processing procedure suggested in the theory section to achieve strict identifiability. We show estimated loading matrices for different sample sizes in simulation case 2 in Figure 7. As  $n$  increases, the posterior mean  $\mathbf{\Lambda}$  converges to the truth, which supports our strict identifiability and posterior consistency results.

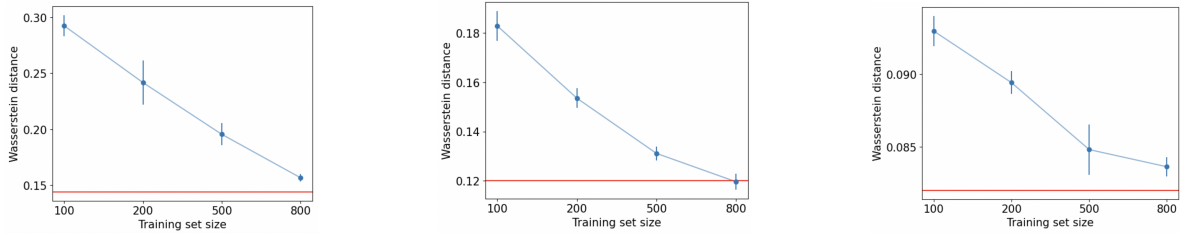


(a) Posterior mean of  $\mathbf{\Lambda}$  for  $n = 100$ . (b) Posterior mean of  $\mathbf{\Lambda}$  for  $n = 800$ . (c) True  $\mathbf{\Lambda}_0$ .

Figure 7: Example results for simulation case 2. Posterior mean of the loading matrix for  $n = 100$  and  $n = 800$  is plotted in (a) and (b), with ground truth in (c).

We evaluate accuracy in characterizing the unknown density of the data using sliced Wasserstein (SW) distance (Bonneel et al., 2015) between test data and data sampled from the posterior predictive. We estimate SW distance using the `pot` python package. We fixed the test sample size to 1,000 to limit Monte Carlo errors in SW distance estimation. As shown in Figure 8, as  $n$  increases, the induced distribution is closer to the true distribution. To provide a reference

“minimum-achievable SW distance”, we show the estimated SW distance between two independently generated test datasets of size 1,000 averaged over 20 replicates as red lines in 8. Due to Monte Carlo error, the minimum-achievable distance is not zero.



(a) Independent non-Gaussian marginal data.

(b) Gaussian linear factor data.

(c) Curved data.

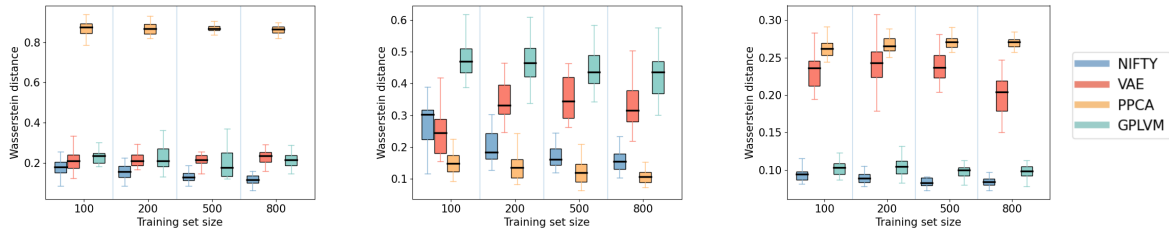
Figure 8: Estimated sliced Wasserstein distance between test data and data from the posterior predictive under NIFTY. The mean and standard deviation for all three experiment settings are shown through a blue error plot. The red horizontal line shows the estimated Wasserstein distance between two identically distributed datasets.

## Comparison with other latent factor models

We implement GP-LVMs, variational autoencoders (VAEs), and Gaussian linear factor models (PPCA) in the same simulated settings and compare performance with NIFTY. Further implementation details are in the Supplementary Materials. Figure 9 shows that NIFTY achieves the smallest out-of-sample sliced Wasserstein distance in most experiments and has the smallest variance across replicates. Meanwhile, PPCA performs remarkably well when data are generated from a Gaussian linear factor model but poorly in non-Gaussian cases. GP-LVM effectively captures non-Gaussianity in panels (a) and (c), and is the second best among the methods. VAE performs comparably with GP-LVM and NIFTY for the 2-dimensional independent data but fails on the curved data.

The latent factors learned by VAE exhibit strong nonlinear relationships, deviating significantly from a standard normal distribution. To provide better visual insight into the results, we plot the first two dimensions of the generated data versus the ground truth in the curved data experiments, shown in Figure 10. PPCA generates Gaussian noise, while VAE and GP-LVM capture the nonlinear relationship between the two dimensions but fail to recover the spread and

variance of the distribution accurately. In contrast, NIFTY accurately recovers the underlying curve and distribution of the data.

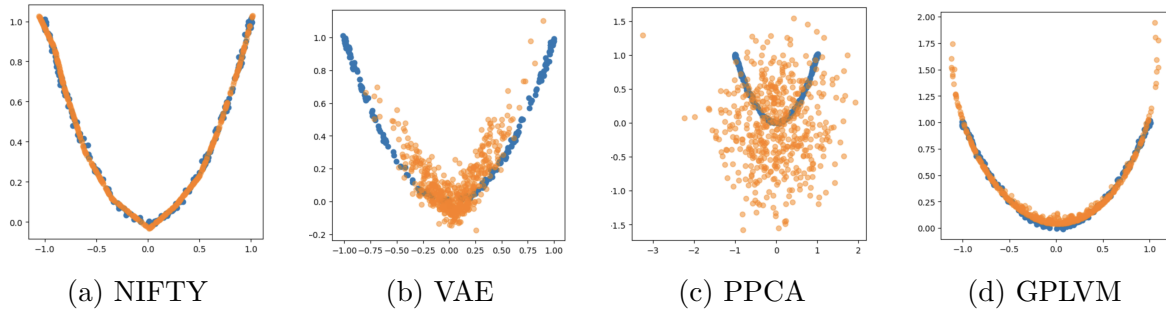


(a) 2-dimensional data generated from independent Gamma and Beta distribution.

(b) 20-dimensional data generated from a Gaussian linear factor.

(c) 10-dimensional data generated from two latent curves.

Figure 9: Box plots of the out-of-sample sliced Wasserstein distance. The three panels respectively display results from the three simulated data sets, and boxes are filled with different colors according to the method.



(a) NIFTY

(b) VAE

(c) PPCA

(d) GPLVM

Figure 10: Comparing out-of-sample data generation in the curved data experiment. The blue curves are from the ground truth, and the orange curves are data points generated by each method. Only the first two dimensions are plotted.

## 5.2 Data visualization with dimension reduction

The latent locations can be viewed as coordinates of the data embedded in low-dimensional unit cubes. When the dimension of the cube is 2 or 3, the latent locations can be naturally used for visualizing high-dimensional data. There is a rich literature on unsupervised dimension reduction algorithms for data visualization, ranging from diffusion maps to the widely popular t-distributed stochastic neighbor embedding (t-SNE) (Van der Maaten and Hinton, 2008)].

Many of the current dimension reduction algorithms for data visualization are uninterpretable black boxes, with an unclear relationship between the low-dimensional coordinates and the orig-

inal high-dimensional data. In fact, it is typically not possible to map back from the low-dimensional coordinates to the observed data space. In contrast, NIFTY has a transparent generative probability model with a loadings matrix that concretely shows the relationship between the low-dimensional factors and the original data. In addition, NIFTY provides uncertainty quantification through a Bayesian approach and we can verify that dimensionality reduction is not leading to a significant loss of information by comparing the empirical distribution of the data to the posterior predictive distribution.

### A Swiss roll embedded in ten-dimensional space

In this example, a three-dimensional Swiss roll is first generated from two independent variables and then embedded in a ten-dimensional space. Starting with  $u_i \sim U(0, 1)$  and  $v_i \sim U(0, 1)$ , we let  $y_i \sim N(\boldsymbol{\mu}, 0.01I_{10})$  with  $\boldsymbol{\mu} = [0, 0, 0, 0, (3\pi u_i + \frac{3}{2}\pi) \sin(3\pi u_i + \frac{3}{2}\pi), (3\pi u_i + \frac{3}{2}\pi) \cos(3\pi u_i + \frac{3}{2}\pi), v_i, 0, 0, 0]^T$ . Figure 11(a) plots the data on the three-dimensional Swiss roll. Figure 11(b) visualizes the two-dimensional representation from diffusion maps. Figure 11(c) shows the inferred latent locations from NIFTY. Both algorithms unfold the roll to a two-dimensional surface, revealing the true generating factors. With NIFTY, we are able to track the transformation from latent factors to data.

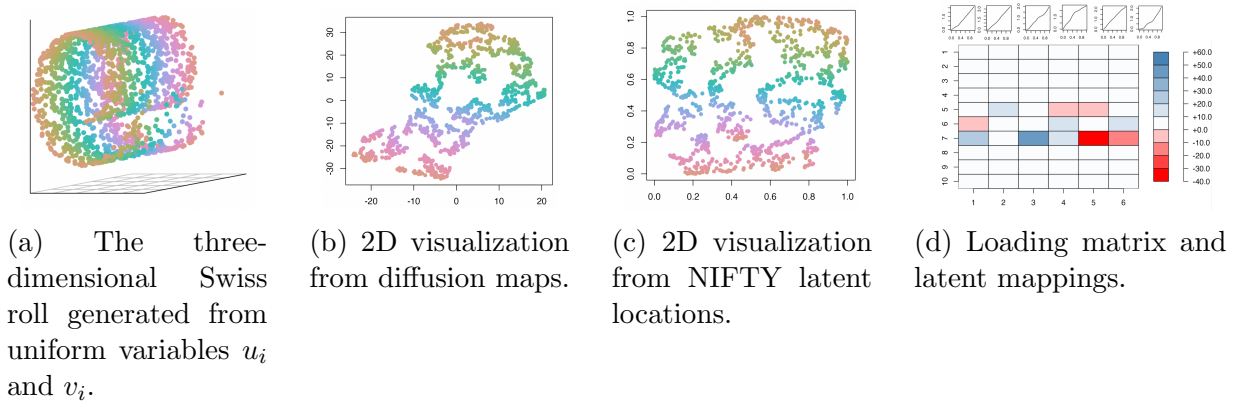


Figure 11: Visualization of a swiss roll embedded in a ten-dimensional space. The scatterplots in panel a-c are colored according to  $v_i$ . We use diffusion maps to generate anchor data and apply NIFTY with  $K = 2$ , and  $H = 6$ . The NIFTY provides an unfolded view of the two latent factors, which is close to the truth. The mapping from latent factors to the data is also accessible.



## Gaussian clusters with heteroscedasticity

We demonstrate a case where NIFTY clearly improves data visualization over the pretraining method. The data are sampled from five Gaussian distributions with different means and variances. The Gaussian means are equally spaced along one axis in a 20-dimensional space, and the variances of each cluster increase from  $1^2$  to  $5^2$ .

From Figure 12(a), we find that diffusion maps are not ideal for visualizing the cluster pattern in a 2D space. As shown in Figure 12(b), t-SNE also does not have ideal performance in this case in only preserving the compact clusters and not capturing the heteroscedasticity. To obtain better visual results, change the pretraining method from diffusion maps to t-SNE. From panel (c) in Figure 12, the latent locations in NIFTY not only display compact cluster patterns but also provide a visual guide about the variance within each cluster. Moreover, the contribution of the dimensions in the data to the low-dimensional representation can be tracked via the loading matrix and nonlinear mappings (panel d).

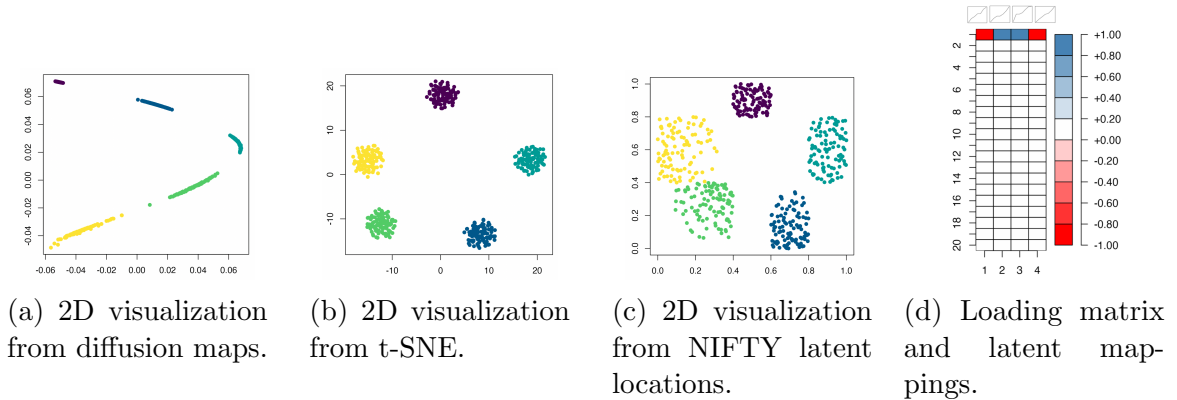
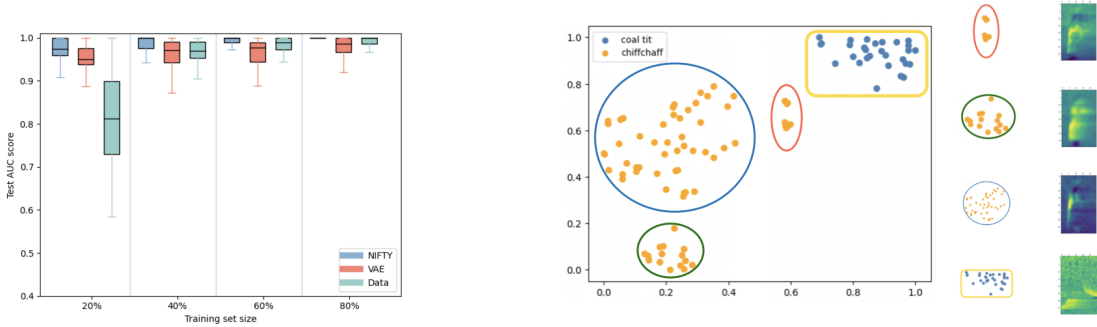


Figure 12: Visualization of 500 points sampled from five 20-dimensional Gaussian with standard deviation being 1, 2, 3, 4, 5, colored according to cluster label (1 to 5 from dark purple to light yellow). Latent locations from NIFTY arguably provide the best visual results, with a clear presentation of cluster patterns and heteroscedasticity between clusters. Besides, the projection from the 2D representation to the data is tractable.

## 6 Audio Classification of Bird Species

In monitoring bird migration and population dynamics, it has become popular to use machine learning for species identification based on recordings of bird vocalizations (Tolkova, 2019). The state-of-the-art in this field relies on deep neural network (DNN) classifiers, which can have excellent performance when large numbers of labeled audio recordings are available for each species (Lehikoinen et al., 2023). Unfortunately, accurate labels of the species vocalizing can be challenging to obtain, particularly for rare species. To address the problem of limited labels in training DNN classifiers, it is common to augment the observed data with fake data (Lauha et al., 2022). For example, one can take the original labeled spectrograms of the bird audio recordings, and for each observed spectrogram generate multiple fake spectrograms that are perturbations. Ideally, these perturbations would mimic real-world variation in bird vocalizations, but in practice, this process tends to be quite ad hoc.

We apply NIFTY to a Finland bird species monitoring study (Lehikoinen et al., 2023) with the goals of improving data augmentation for downstream DNN classifiers or alternatively directly using NIFTY for classification based on limited training data. By training NIFTY on available spectrogram data from a species of interest, we can learn lower dimensional structure in the data and exploit this structure in generating new spectrograms representative of the variation in calls from a given species. This should provide a more accurate approach for generating new spectrograms that are close to the limited available training data for use in data augmentation for DNNs. Current practice adds an arbitrary amount of noise, shifts the spectrogram image slightly, and/or masks some of the data (Salamon and Bello, 2017).



(a) Comparing classification accuracy in terms of AUC using latent factors learned from NIFTY and VAE against using an SVM with the vectorized spectrogram data.

(b) 2D visualization from the NIFTY latent locations and a zoom-in view of the sub-clusters within common chiffchaff.

Figure 13: Left: classification accuracy using latent factors learned from NIFTY, VAE, and using an SVM with the vectorized spectrogram data. Test classification accuracy in terms of AUC under the ROC curve is displayed as the training set varies from 20% to 80% of the dataset. We have 102 data points with labels, consisting of 73 chiffchaff calls and 29 coal tit calls. The number of latent factors is five for both NIFTY and VAE. Right: 2D visualization of NIFTY latent locations. Locations are colored according to the true species identity - either chiffchaff or coal tit. There are distinct clusters for the species. For the common chiffchaff, we also see sub-clusters. The zoom-in view of each sub-cluster provides information about different call types within one species.

## 6.1 Data augmentation to increase training samples

We pre-process the audio files by clipping the songs into syllables according to manual labels, then convert them to spectrograms by applying windowing and the fast Fourier transform (FFT). As a result, each clip of data  $\mathbf{S}_i$  is a  $M \times T$  spectrogram, with each entry  $S_{i[mt]}$  encoding power within the  $m$ th frequency band at discrete time point  $t$ . In our examples,  $M = 120$  and  $T = 25$ . From Figure 13(b), bird calls within a species share similar shapes or vary from several call types. That allows us to represent the  $120 \times 25$ -dimensional spectrogram by mapping from a few factors.

We apply NIFTY to calls from the common chiffchaff, a migratory warbler that lives in Europe, Asia, and northern Africa. The data include  $N = 73$  collected samples of spectrograms, and each vectorized spectrogram has  $P = 3000$ . Through pretraining using diffusion maps, we choose five anchor dimensions. After running NIFTY, we can generate new latent locations from

Unif[0, 1]<sup>5</sup> and apply the learned mappings and loading matrix. Figure 14 shows generated new data around one clip of a call from the common chiffchaff obtained by adding a small random perturbation to the latent location inferred for that clip. One can tune the deviation of generated data from the original data by varying the magnitude of added noise to make it closer or further from a specific bird call. The figure shows what happens to the spectrogram as we increase the amount of perturbation of the latent location for VAE and for NIFTY. We find that NIFTY produces spectrograms that maintain the key attributes of the original bird call, while VAEs become degraded by noise.

We also generate 100 new song clips using NIFTY and VAE, by sampling latent factors from the assumed distribution and applying the transformation. The sound clips, along with original calls, are available on <https://nifty-master.github.io/>. There are occasionally strong noises in the VAE generated calls, and some clips are unlike bird calls (e.g. the call at the 9th second), while NIFTY generates more realistic variations.

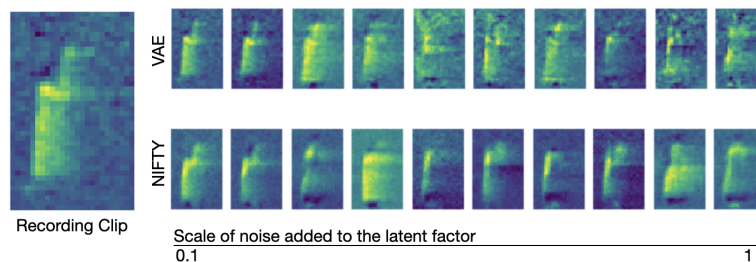


Figure 14: Comparing data generation performance between NIFTY and VAE for the common chiffchaff. VAE’s output becomes more noisy as added noise increases, but NIFTY’s output remains near the underlying manifold.

## 6.2 Classification based on latent factors

Most existing bird acoustic monitoring frameworks are built on large-scale data and neural-net-based classifiers trained on labeled birdsong recordings, such as the BirdNet (Kahl et al., 2021). Such algorithms can be very accurate but require lots of labeled data for each bird species, collected under different conditions in terms of distance from the microphone, background noise, etc. There is a need for accurate classifiers that are less data-hungry, motivating the use of

NIFTY in this context.

We demonstrate the potential of NIFTY focusing on binary classification between the common chiffchaff and the coal tit. The coal tit is a slightly larger bird inhabiting an overlapping range. Letting  $y_i \in \{-1, 1\}$  denote the label of data  $\mathbf{x}_i$ , we apply a simple support vector machine (SVM) classifier (Cortes and Vapnik, 1995), which learns a hyperplane  $\mathbf{w}\mathbf{x} + \mathbf{b} = 0$  to separate the two species. Formally, we solve an optimization problem  $\min_{\mathbf{w}, \mathbf{b}} \|\mathbf{w}\|$  such that  $y_i(\mathbf{w}\mathbf{x}_i + \mathbf{b}) > 0$  for all  $i = 1, \dots, N$ . As shown in Figure 13(a), fitting such a classifier on the high-dimensional data results in low accuracy in predicting the label. Therefore, we use the low-dimensional factors  $\boldsymbol{\eta}_i$  learned from NIFTY to fit an SVM instead of  $\mathbf{x}_i$ , which drastically enhances accuracy, especially when the sample size is small. Additionally, we compare with using a VAE to generate low-dimensional features for the classification model. Applying first-stage dimension reduction with either NIFTY or VAE leads to much better performance in small training-size cases. Across the different training sample sizes, NIFTY has consistently better performance than VAEs. The 2D visualization (panel b) of the common chiffchaff vocalizations displays sub-cluster patterns, which are as expected given the variation in vocalization types. The audio clips of each sub-cluster are also available on the sound webpage <https://nifty-master.github.io/>.

Overall, we find that NIFTY generates more realistic data augmentation and improves classification accuracy when the number of labels is limited, bypassing the need for a much more complex and data-hungry DNN.

## 7 Discussion

The focus of this article is on introducing a relatively simple latent variable modeling framework for identifiable and interpretable dimensionality reduction, with sufficient flexibility to characterize complex data. We illustrated this flexibility in building realistic generative models for bird vocalization data. The proposed framework represents an appealing competitor to popu-

lar GP-LVM and VAE approaches. Building on our initial developments for NIFTY, there are several natural next steps. First, we can accommodate observed data  $\mathbf{x}_i$  that have a variety of measurement scales, including binary, categorical, count and continuous, through one of two simple modifications. One direction is to define a Gaussian linear factor model for underlying data  $\mathbf{x}_i^*$  and then let  $x_{ij} = h_j(x_{ij}^*)$  with  $h_j(\cdot)$  an appropriate link function for the  $j$ th variable type. Another is to define each  $x_{ij}$  as belonging to an exponential family including the latent factors as predictors in a generalized linear model (GLM). In both cases, it is of interest to consider alternatives to the MCMC-based Bayesian inference approach of this paper including pure optimization approaches for rapid dimension reduction and variational approximations to speed up Bayesian analyses.

Another interesting direction forward is to carefully consider the role of pretraining in the practical performance and theoretical properties of NIFTY. While we focused on manifold learning algorithms for pretraining, such as diffusion maps, it would be appealing to be able to adaptively select the type of pretraining most appropriate for the data at hand. For example, some data may have a lower-dimensional manifold structure, while other data may be more appropriately characterized as a stratified space.

One contribution in this paper that is of considerable independent interest beyond the specific factor structure of NIFTY is our highlighting of the important problem of latent variable *distributional shift*. We proposed a particular strategy to deal with distribution shift in our inferences, but a careful study of when and why such shifts occur and how they can be optimally handled remain open problems.

There are many additional natural next extensions of NIFTY. For example, there has been considerable interest in recent work in using factor models for multi-study (De Vito et al., 2021) and multi-type data. Even in the Gaussian linear factor case, interesting challenges arise in inferring study-specific versus shared factors (Chandra et al., 2023). By extending the NIFTY structure to such settings, we enable considerable gains in flexibility over the state of the art,

while maintaining identifiability.

## References

- Allman, E. S., C. Matias, and J. A. Rhodes (2009). Identifiability of Parameters in Latent Structure Models With Many Observed Variables. *The Annals of Statistics* 37, 3099–3132.
- Arminger, G. and B. O. Muthén (1998). A Bayesian Approach to Nonlinear Latent Variable Models Using the Gibbs Sampler and the Metropolis-Hastings Algorithm. *Psychometrika* 63, 271–300.
- Arora, S., R. Ge, Y. Halpern, D. Mimno, A. Moitra, D. Sontag, Y. Wu, and M. Zhu (2013). A Practical Algorithm for Topic Modeling With Provable Guarantees. In *International Conference on Machine Learning*, pp. 280–288. PMLR.
- Bhattacharya, A. and D. B. Dunson (2011). Sparse Bayesian Infinite Factor Models. *Biometrika* 98(2), 291–306.
- Bing, X., F. Bunea, Y. Ning, and M. Wegkamp (2020). Adaptive estimation in structured factor models with applications to overlapping clustering. *The Annals of Statistics* 48(4), 2055 – 2081.
- Bodelet, J. and J. Shan (2020). Nonparametric Additive Factor Models. *arXiv Preprint arXiv:2003.13119*.
- Bonneel, N., J. Rabin, G. Peyré, and H. Pfister (2015). Sliced and Radon Wasserstein Barycenters of Measures. *Journal of Mathematical Imaging and Vision* 51, 22–45.
- Carvalho, C. M., J. Chang, J. E. Lucas, J. R. Nevins, Q. Wang, and M. West (2008). High-Dimensional Sparse Factor Modeling: Applications in Gene Expression Genomics. *Journal of the American Statistical Association* 103(484), 1438–1456.

- Chandra, N. K., A. Canale, and D. B. Dunson (2023). Escaping the Curse of Dimensionality in Bayesian Model-Based Clustering. *Journal of Machine Learning Research* 24, 144–1.
- Chandra, N. K., D. B. Dunson, and J. Xu (2023). Inferring Covariance Structure from Multiple Data Sources via Subspace Factor Analysis. *arXiv preprint arXiv:2305.04113*.
- Coifman, R. R. and S. Lafon (2006). Diffusion Maps. *Applied and Computational Harmonic Analysis* 21(1), 5–30.
- Comon, P. (1994). Independent Component Analysis, a New Concept? *Signal Processing* 36(3), 287–314.
- Cortes, C. and V. Vapnik (1995). Support-vector Networks. *Machine learning* 20, 273–297.
- Creswell, A., T. White, V. Dumoulin, K. Arulkumaran, B. Sengupta, and A. A. Bharath (2018). Generative Adversarial Networks: An Overview. *IEEE Signal Processing Magazine* 35(1), 53–65.
- Dai, B., Z. Wang, and D. Wipf (2020). The Usual Suspects? Reassessing Blame for VAE Posterior Collapse. In *International Conference on Machine Learning*, pp. 2313–2322. PMLR.
- De Vito, R., R. Bellio, L. Trippa, and G. Parmigiani (2021). Bayesian Multistudy Factor Analysis for High-throughput Biological Data. *The Annals of Applied Statistics* 15(4), 1723–1741.
- Duan, L. L., A. L. Young, A. Nishimura, and D. B. Dunson (2020). Bayesian Constraint Relaxation. *Biometrika* 107(1), 191–204.
- Dunson, D. B. and N. Wu (2021). Inferring Manifolds From Noisy Data Using Gaussian Processes. *arXiv Preprint arXiv:2110.07478*.
- Fruchter, B. (1954). *Introduction to Factor Analysis*. Van Nostrand Series in Psychology.
- Ghahramani, Z., G. E. Hinton, et al. (1996). The EM Algorithm for Mixtures of Factor Analyzers. Technical report, Technical Report CRG-TR-96-1, University of Toronto.



- Ghosal, S., J. K. Ghosh, and R. Ramamoorthi (1999). Posterior Consistency of Dirichlet Mixtures in Density Estimation. *The Annals of Statistics* 27(1), 143–158.
- Ghosal, S. and A. Van der Vaart (2017). *Fundamentals of Nonparametric Bayesian Inference*, Volume 44. Cambridge University Press.
- Ghosh, J. and D. B. Dunson (2009). Default Prior Distributions and Efficient Posterior Computation in Bayesian Factor Analysis. *Journal of Computational and Graphical Statistics* 18(2), 306–320.
- Gibson, W. (1960). Nonlinear Factors in Two Dimensions. *Psychometrika* 25(4), 381–392.
- Harman, H. H. (1976). *Modern Factor Analysis*. University of Chicago Press.
- Kahl, S., C. M. Wood, M. Eibl, and H. Klinck (2021). BirdNET: A Deep Learning Solution for Avian Diversity Monitoring. *Ecological Informatics* 61, 101236.
- Kingma, D. P. and M. Welling (2014). Stochastic Gradient VB and the Variational Auto-Encoder. In *Second International Conference on Learning Representations, ICLR*, Volume 19, pp. 121.
- Kobyzev, I., S. J. Prince, and M. A. Brubaker (2020). Normalizing Flows: An Introduction and Review of Current Methods. *IEEE Transactions on Pattern Analysis and Machine Intelligence* 43(11), 3964–3979.
- Kolouri, S., S. R. Park, M. Thorpe, D. Slepcev, and G. K. Rohde (2017). Optimal Mass Transport: Signal Processing and Machine-Learning Applications. *IEEE Signal Processing Magazine* 34(4), 43–59.
- Lauha, P., P. Somervuo, P. Lehtikoinen, L. Geres, T. Richter, S. Seibold, and O. Ovaskainen (2022). Domain-specific Neural Networks Improve Automated Bird Sound Recognition Already with Small Amount of Local Data. *Methods in Ecology and Evolution* 13(12), 2799–2810.

- Legramanti, S., D. Durante, and D. B. Dunson (2020). Bayesian Cumulative Shrinkage for Infinite Factorizations. *Biometrika* 107(3), 745–752.
- Lehikoinen, P., M. Rannisto, U. Camargo, A. Aintila, P. Lauha, E. Piirainen, P. Somervuo, and O. Ovaskainen (2023). A Successful Crowdsourcing Approach for Bird Sound Classification. *Citizen Science* 8(1).
- Li, P. and S. Chen (2016). A Review on Gaussian Process Latent Variable Models. *CAAI Transactions on Intelligence Technology* 1(4), 366–376.
- Lopes, H. F. and M. West (2004). Bayesian Model Assessment in Factor Analysis. *Statistica Sinica*, 41–67.
- Makalic, E. and D. F. Schmidt (2015). A Simple Sampler for the Horseshoe Estimator. *IEEE Signal Processing Letters* 23(1), 179–182.
- McDonald, R. P. (1962). A General Approach to Nonlinear Factor Analysis. *Psychometrika* 27(4), 397–415.
- McLachlan, G. J., D. Peel, and R. W. Bean (2003). Modelling High-Dimensional Data by Mixtures of Factor Analyzers. *Computational Statistics & Data Analysis* 41(3-4), 379–388.
- Merkle, E. C. and Y. Rosseel (2015). Blavaan: Bayesian Structural Equation Models via Parameter Expansion. *arXiv Preprint arXiv:1511.05604*.
- Montanari, A. and C. Viroli (2010). Heteroscedastic Factor Mixture Analysis. *Statistical Modelling* 10(4), 441–460.
- Moran, G. E., D. Sridhar, Y. Wang, and D. Blei (2022). Identifiable Deep Generative Models via Sparse Decoding. *Transactions on Machine Learning Research* (2835-8856).
- Murray, J. S., D. B. Dunson, L. Carin, and J. E. Lucas (2013). Bayesian Gaussian Copula Factor Models for Mixed Data. *Journal of the American Statistical Association* 108(502), 656–665.

- Papastamoulis, P. and I. Ntzoufras (2022). On the Identifiability of Bayesian Factor Analytic Models. *Statistics and Computing* 32(2), 23.
- Poworoznek, E., F. Ferrari, and D. Dunson (2021). Efficiently Resolving Rotational Ambiguity in Bayesian Matrix Sampling With Matching. *arXiv Preprint arXiv:2107.13783*.
- Rezende, D. J., S. Mohamed, and D. Wierstra (2014). Stochastic Backpropagation and Variational Inference in Deep Latent Gaussian Models. In *International Conference on Machine Learning*, Volume 2, pp. 2.
- Roberts, G. O. and O. Stramer (2002). Langevin Diffusions and Metropolis-Hastings Algorithms. *Methodology and Computing in Applied Probability* 4, 337–357.
- Roberts, G. O. and R. L. Tweedie (1996). Exponential Convergence of Langevin Distributions and Their Discrete Approximations. *Bernoulli*, 341–363.
- Salamon, J. and J. P. Bello (2017). Deep Convolutional Neural Networks and Data Augmentation for Environmental Sound Classification. *IEEE Signal Processing Letters* 24(3), 279–283.
- Sardy, S. and M.-P. Victoria-Feser (2012). Isotone Additive Latent Variable Models. *Statistics and Computing* 22, 647–659.
- Shan, S. and I. Daubechies (2022). Diffusion Maps: Using the Semigroup Property for Parameter Tuning. In *Theoretical Physics, Wavelets, Analysis, Genomics: An Interdisciplinary Tribute to Alex Grossmann*, pp. 409–424. Springer.
- Song, X.-Y. and Z.-H. Lu (2012). Semiparametric Transformation Models With Bayesian P-Splines. *Statistics and Computing* 22, 1085–1098.
- Titsias, M. and N. D. Lawrence (2010). Bayesian Gaussian Process Latent Variable Model. In *Proceedings of the Thirteenth International Conference on Artificial Intelligence and Statistics*, pp. 844–851. JMLR Workshop and Conference Proceedings.

- Tolkova, I. (2019). Feature Representations for Conservation Bioacoustics: Review and Discussion. *Harvard University*.
- Van der Maaten, L. and G. Hinton (2008). Visualizing Data Using t-SNE. *Journal of Machine Learning Research* 9(11).
- Wang, Y., D. Blei, and J. P. Cunningham (2021). Posterior Collapse and Latent Variable Non-Identifiability. *Advances in Neural Information Processing Systems* 34, 5443–5455.
- Wellner, J. et al. (2013). *Weak Convergence and Empirical Processes: With Applications to Statistics*. Springer Science & Business Media.
- Yalcin, I. and Y. Amemiya (2001). Nonlinear Factor Analysis as a Statistical Method. *Statistical Science*, 275–294.

## A Funding

This project has received funding from the European Research Council (ERC) under the European Union’s Horizon 2020 research and innovation programme (grant agreement No 856506), United States National Institutes of Health (R01ES035625), Office of Naval Research (N00014-21-1-2510), and National Institute of Environmental Health Sciences (P42-ES010356, R01-AI155733, R01-ES027498).

## B Proofs

### Proof of Proposition 1

*Proof.* Let  $F_k^0(u)$  denote the CDF of the prior for  $u_{ik}$  defined in (4) and  $F_k^N(u)$  denote the corresponding empirical CDF with  $N$  data points. By the definition of a Wasserstein-2 distance,

when  $\nu \rightarrow \infty$ , the  $i$ th order statistics of  $\mathbf{u}_{\cdot k}$  converge in probability to  $i/N$ . Hence for any  $\epsilon > 0$  and any  $u \in [0, 1]$ , there exists an  $M$  large enough, such that

$$\text{pr}(|F_k^M(u) - u| \geq \epsilon) = \text{pr}(|i/M - u| \geq \epsilon) \rightarrow 0, \text{ as } \nu \rightarrow \infty,$$

with  $i$  chosen such that  $u_{(i-1)k} < u < u_{(i)k}$  with  $u_{(1)k}, \dots, u_{(M)k}$  the order statistics of  $u_{1k}, \dots, u_{Mk}$ . As  $N \rightarrow \infty$ , the distance between empirical CDF and true CDF converges to zero. Therefore, under prior specification (4),

$$F_k^0(u) \rightarrow u.$$

□

## Proof of Theorem 1

*Proof.* We prove the identifiability results in three parts: first the strict identifiability of latent locations  $u_{ik}$ s, then the strict identifiability of  $\Sigma$ , and finally the generic identifiability of  $\Lambda$  and  $\mathbf{g}$ .

### Identifiability of latent locations

Under Assumption 3, the value of  $\sigma_{j_1}^2, \dots, \sigma_{j_K}^2$  are known or estimated in advance. In Assumption (1), the  $k$ th anchor dimension depends only the factor  $h_k$ . Identifiability of  $u_{ik}$  can be described as: for each  $k = 1, \dots, K$ , if two sets of parameters  $(u_{ik}, g_{h_k}, \lambda_{jh_k})$  and  $(u'_{ik}, g'_{h_k}, \lambda'_{jh_k})$  yield the same likelihood for  $x_{ij_k}$ , then we must have  $u_{ik} = u'_{ik}$  or  $u_{ik} = 1 - u'_{ik}$ . Further, there is a constant  $c$  such that  $g_{h_k}(u) = cg'_{h_k}(u)$  for any  $u \in [0, 1]$  and  $\lambda_{jh_k} = 1/c\lambda'_{jh_k}$ .

Since the log-likelihood of the two sets of parameters should be equal, we have

$$[x_{ij_k} - \lambda_{jh_k}g_{h_k}(u_{ik})]^2/\sigma_{j_k}^2 = [x_{ij_k} - \lambda'_{jh_k}g'_{h_k}(u'_{ik})]^2/\sigma_{j_k}^2.$$

Furthermore,

$$\lambda_{jh_k}^2 g_{h_k}(u_{ik})^2 - (\lambda'_{jh_k})^2 g'_{h_k}(u'_{ik})^2 - x_{ij_k} [\lambda_{jh_k} g_{h_k}(u_{ik}) - \lambda'_{jh_k} g'_{h_k}(u'_{ik})] = 0$$

holds for any value of  $x_{ij_k}$ , and therefore we must have  $\lambda_{jh_k} g_{h_k}(u_{ik}) = \lambda'_{jh_k} g'_{h_k}(u'_{ik})$ . Since  $g_h$  are monotonely increasing functions from  $[0, 1]$  to  $\mathbb{R}$ , the inverse exists and

$$u_{ik} = g_{h_k}^{-1}[\lambda_{jh_k}^{-1} \lambda'_{jh_k} g'_{h_k}(u'_{ik})].$$

If  $\lambda_{jh_k} \lambda'_{jh_k} > 0$ , since both  $g_h^{-1}$  and  $g'_h$  are monotonely non-decreasing functions for every  $h$ ,  $g_{h_k}^{-1} \circ \lambda_{jh_k}^{-1} \lambda'_{jh_k} g'_{h_k}$  is also a non-decreasing function. Actually, it is an identity function, because

$$\begin{aligned} t = \text{pr}(u_{ik} \leq t) &= \text{pr}(g_{h_k}^{-1}[\lambda_{jh_k}^{-1} \lambda'_{jh_k} g'_{h_k}(u'_{ik})] \leq t) \\ &= \text{pr}(u'_{ik} \leq (g_{h_k}^{-1} \circ \lambda_{jh_k}^{-1} \lambda'_{jh_k} g'_{h_k})^{-1}(t)) = (g_{h_k}^{-1} \circ \lambda_{jh_k}^{-1} \lambda'_{jh_k} g'_{h_k})^{-1}(t). \end{aligned}$$

Similarly, when  $\lambda_{jh_k} \lambda'_{jh_k} < 0$ , we have  $u_{ik} = 1 - u'_{ik}$ . Furthermore, we show that  $g_{h_k}^{-1} \circ \lambda_{jh_k}^{-1} \lambda'_{jh_k} g'_{h_k}$  is an identity function or  $-g_{h_k}^{-1} \circ \lambda_{jh_k}^{-1} \lambda'_{jh_k} g'_{h_k}$  is an identity function.

### Identifiability of residual covariance

As  $\Sigma$  is diagonal, it suffices to show identifiability of the diagonal elements  $\sigma_j^2$ . For ease of notation, we denote the  $j$ th element in  $\Lambda \boldsymbol{\eta}_i$  being a map from  $\mathbf{u}_i$  as  $m(\mathbf{u}_i)$ . Since we have shown identifiability of  $\mathbf{u}_i$ , it suffices to show: if there exists  $m, m'$  and  $\sigma_j^2, (\sigma'_j)^2$  such that

$$\frac{[x_{ij} - m(\mathbf{u}_i)]^2}{\sigma_j^2} = \frac{[x_{ij} - m'(\mathbf{u}_i)]^2}{(\sigma'_j)^2}, \forall x_{ij},$$

then one must have  $x_{ij} = \left(\frac{1}{\sigma_j^2} - \frac{1}{(\sigma'_j)^2}\right)^{-1} \left(\frac{m(\mathbf{u}_i)}{\sigma_j^2} - \frac{m'(\mathbf{u}_i)}{(\sigma'_j)^2}\right)$  or  $x_{ij} = \left(\frac{1}{\sigma_j^2} + \frac{1}{(\sigma'_j)^2}\right)^{-1} \left(\frac{m(\mathbf{u}_i)}{\sigma_j^2} + \frac{m'(\mathbf{u}_i)}{(\sigma'_j)^2}\right)$ .

With  $\sigma_j^2 \neq (\sigma'_j)^2$ , either equation will give a contradiction because  $\mathbf{u}_i$  is a latent location vector specified by the anchor dimensions, but  $x_{ij}$  can take any value. Therefore, we must have

$$\sigma_j^2 = (\sigma'_j)^2.$$

## Identifiability of loadings and factors

Without loss of generality, we assume that  $\lambda_{jh_k} \lambda'_{jh_k} > 0$  and hence  $u_{ik}$  are identifiable for all  $k$ . Supposing there is another set of parameters  $(\mathbf{\Gamma}, \mathbf{e})$  yielding the same likelihood as  $(\mathbf{\Lambda}, \mathbf{g})$ , we will show that there is a linear transformation between  $\mathbf{\Gamma}$  and  $\mathbf{\Lambda}$  within the  $k$ th block.

We first show there exists a reversible linear transformation  $\mathbf{T} \in \mathbb{R}^{H \times H}$ , such that  $\mathbf{\Gamma} = \mathbf{\Lambda} \mathbf{T}$  and  $\mathbf{e}(\mathbf{u}) = \mathbf{T}^{-1} \mathbf{g}(\mathbf{u})$  for any value of  $\mathbf{u} \in [0, 1]^K$ . Recall that in our model, columns in  $\mathbf{\Gamma}$  and functions in  $\mathbf{e}$  can be rearranged so that they can be written in partition  $\mathbf{\Gamma}^1, \dots, \mathbf{\Gamma}^K$  and  $\mathbf{e}^1, \dots, \mathbf{e}^K$  using the same criteria when partitioning  $\mathbf{\Lambda}$  and  $\mathbf{g}$ . Since  $u_{ik}$  are uniquely determined by the anchor dimension, we have

$$[\mathbf{\Gamma}^1 \mathbf{e}^1(u_{i1}), \dots, \mathbf{\Gamma}^K \mathbf{e}^K(u_{iK})] = [\mathbf{\Lambda}^1 \mathbf{g}^1(u_{i1}), \dots, \mathbf{\Lambda}^K \mathbf{g}^K(u_{iK})],$$

or omit some subscripts,  $\mathbf{\Gamma} \mathbf{e}(\mathbf{u}) = \mathbf{\Lambda} \mathbf{g}(\mathbf{u})$ . Since both matrices are of full column rank, there exists a  $\mathbf{B}$  matrix to make  $\mathbf{B} \mathbf{\Lambda} = \mathbf{I}$  and therefore  $\mathbf{g}(\mathbf{u}) = \mathbf{B} \mathbf{\Gamma} \mathbf{e}(\mathbf{u})$  for every  $\mathbf{u}$ . Let  $\mathbf{T} = \mathbf{B} \mathbf{\Lambda}$  denote the transformation between  $\mathbf{g}$  and  $\mathbf{e}$ , then we also have  $\mathbf{\Gamma} = \mathbf{\Lambda} \mathbf{T}$ .

Next, we prove that  $\mathbf{T}$  is a block diagonal matrix, with blocks divided by the  $K$  partitions. Note that  $\mathbf{T}[e_1(u_{ik_1}), \dots, e_H(u_{ik_H})]^T = [g_1(u_{ik_1}), \dots, g_H(u_{ik_H})]^T$ . If  $\mathbf{T}$  is not a block diagonal matrix, assume that  $\mathbf{T}_{h_1 h_2} \neq 0$  and that  $k_{h_1} = 1, k_{h_2} = 2$ . Then  $g_{h_1}(u_{i1})$  must be a linear combination of  $e_{h_1}(u_{i1})$  and  $e_{h_2}(u_{i2})$ , for any  $u_{i1}$  and  $u_{i2}$ , which violates the definition of  $g_{h_1}$ . Therefore  $\mathbf{T}_{h_1 h_2} = 0$  if  $k_{h_1} \neq k_{h_2}$ ; hence  $\mathbf{T}$  is a block diagonal matrix.  $\square$

## Proof of Theorem 2

*Proof.* Let  $L_{\Theta^0}^N(\mathbf{x})$  denote the likelihood of  $(\mathbf{x}_1, \dots, \mathbf{x}_N)$  under parameters  $\Theta^0 = \Lambda^0, g^0, \Sigma^0$ , and  $L_{\Theta}^N(\mathbf{x})$  be the likelihood under parameters  $\Theta = \Lambda, g, \Sigma$ . By generic identifiability, the subset of

$\Theta$  satisfying  $L_{\Theta}^N(\mathbf{x}) = L_{\Theta^0}^N(\mathbf{x})$  has measure zero. Therefore, for any  $\epsilon > 0$ , there must exist a  $\delta_{\epsilon, N} > 0$  such that the prior  $\Pi$  for  $\Theta$  satisfies

$$\lim_{N \rightarrow \infty} \Pi [\mathcal{N}_{\epsilon}^C(\Theta^0) \cap \{|L_{\Theta^0}^N(\mathbf{x}) - L_{\Theta}^N(\mathbf{x})| < \delta_{\epsilon, N}\}] = 0.$$

We can define tests  $\psi^N := 1\{|L_{\Theta^0}^N(\mathbf{x}) - L_{\Theta}^N(\mathbf{x})| \geq \delta_{\epsilon, N}\}$  with  $\mathbb{P}_0^N \psi^N \rightarrow 0$  and  $\sup_{\Theta^0 \in \mathcal{N}_{\epsilon}^C(\Theta^0)} \mathbb{P}_{\Theta}^N(1 - \psi^N) \rightarrow 0$ . Applying Schwartz's theorem (theorem 6.16 in Ghosal and Van der Vaart (2017)), the posterior of the model parameters is strongly consistent at  $\Theta^0$ .  $\square$

### Proof of Theorem 3

*Proof.* Let  $f_{\Lambda, \mathbf{g}, \Sigma}$  denote the induced density of  $\mathbf{x}_i$  given  $(\Lambda, \mathbf{g}, \Sigma)$  and  $f^0$  the true data-generating density having parameters  $(\Lambda^0, \mathbf{g}^0, \Sigma^0)$ . By definition, the KL divergence between  $f_{\Lambda, \mathbf{g}, \Sigma}, f^0$  is

$$KL(f_{\Lambda, \mathbf{g}, \Sigma}, f^0) = \int f^0(\mathbf{x}) \log \frac{f^0(\mathbf{x})}{f_{\Lambda, \mathbf{g}, \Sigma}(\mathbf{x})} d\mathbf{x}. \quad (7)$$

Suppose  $\Sigma^0 = \text{diag}[(\sigma_1^0)^2, \dots, (\sigma_P^0)^2]$  and  $\Sigma = \text{diag}(\sigma_1^2, \dots, \sigma_P^2)$ . Then, we introduce diagonal matrix  $\Gamma = \text{diag}\left[\frac{\sigma_1^2}{(\sigma_1^0)^2}, \dots, \frac{\sigma_P^2}{(\sigma_P^0)^2}\right]$ , and represent  $\Sigma = \Gamma^{1/2} \Sigma^0 \Gamma^{1/2}$ . We have

$$\begin{aligned} \frac{f_{\Lambda^0, \mathbf{g}^0, \Sigma^0}(\mathbf{x}_i)}{f_{\Lambda^0, \mathbf{g}^0, \Sigma}(\mathbf{x}_i)} &= \frac{\int_{[0,1]^H} \phi_{\Sigma^0}[\mathbf{x}_i - \Lambda^0 \mathbf{g}^0(\mathbf{u}_i)] d\mathbf{u}_i}{\int_{[0,1]^H} \phi_{\Sigma}[\mathbf{x}_i - \Lambda^0 \mathbf{g}^0(\mathbf{u}_i)] d\mathbf{u}_i} \\ &= \exp \left\{ \frac{1}{2} (\mathbf{x}_i \Gamma^{-1/2} - \mathbf{x}_i)^T (\Sigma^0)^{-1} (\mathbf{x}_i \Gamma^{-1/2} - \mathbf{x}_i) \right\}, \end{aligned}$$

which goes to 1 as  $\|\Sigma - \Sigma^0\|_{\infty} \rightarrow 0$ . On the other hand,

$$\begin{aligned} \frac{f_{\Lambda^0, \mathbf{g}^0, \Sigma}(\mathbf{x}_i)}{f_{\Lambda, \mathbf{g}, \Sigma}(\mathbf{x}_i)} &= \frac{\int_{[0,1]^H} \phi_{\Sigma}[\mathbf{x}_i - \Lambda^0 \mathbf{g}^0(\mathbf{u}_i)] d\mathbf{u}_i}{\int_{[0,1]^H} \phi_{\Sigma}[\mathbf{x}_i - \Lambda \mathbf{g}(\mathbf{u}_i)] d\mathbf{u}_i} \\ &\leq \sup_{\mathbf{u}_i \in [0,1]^H} \exp \left\{ \frac{1}{2} [\Lambda \mathbf{g}(\mathbf{u}_i) - \Lambda^0 \mathbf{g}^0(\mathbf{u}_i)]^T \Sigma^{-1} [\Lambda \mathbf{g}(\mathbf{u}_i) - \Lambda^0 \mathbf{g}^0(\mathbf{u}_i)] \right. \\ &\quad \left. - \frac{1}{2} [\mathbf{x}_i - \Lambda^0 \mathbf{g}^0(\mathbf{u}_i)]^T \Sigma^{-1} [\Lambda \mathbf{g}(\mathbf{u}_i) - \Lambda^0 \mathbf{g}^0(\mathbf{u}_i)] \right\}, \end{aligned}$$



which goes to 1 as  $\|\Lambda^0 \mathbf{g}^0 - \Lambda \mathbf{g}\|_\infty \rightarrow 0$ . With similar derivation on  $\frac{f_{\Lambda, \mathbf{g}, \Sigma}(\mathbf{x})}{f_{\Lambda^0, \mathbf{g}^0, \Sigma^0}(\mathbf{x})}$ , we have  $\log \frac{f^0(\mathbf{x})}{f_{\Lambda, \mathbf{g}, \Sigma}(\mathbf{x})} \rightarrow 0$  as  $\|\Lambda^0 \mathbf{g}^0 - \Lambda \mathbf{g}\|_\infty \rightarrow 0$ . Under Assumption 4,  $\frac{f^0(\mathbf{x})}{f_{\Lambda, \mathbf{g}, \Sigma}(\mathbf{x})}$  has a finite upper bound. Therefore we can apply the dominated convergence theorem, and obtain

$$KL(f_{\Lambda, \mathbf{g}, \Sigma}, f^0) = \int f^0(\mathbf{x}) \log \frac{f^0(\mathbf{x})}{f_{\Lambda, \mathbf{g}, \Sigma}(\mathbf{x})} d\mathbf{x} \rightarrow 0$$

as  $\|\Lambda^0 \mathbf{g}^0 - \Lambda \mathbf{g}\|_\infty \rightarrow 0$  and  $\|\Sigma - \Sigma^0\|_\infty \rightarrow 0$ .

Therefore, for an arbitrary  $\epsilon > 0$  bounding the KL divergence from  $f^0$ , we can find corresponding scalars  $\delta_{\Lambda, \epsilon}, \delta_{\mathbf{g}, \epsilon}, \delta_{\Sigma, \epsilon} > 0$  bounding sup-norm neighborhoods for the respective model parameters. As long as  $\Lambda$  is in the  $\delta_{\Lambda, \epsilon}$ -sup-norm neighborhood of  $\Lambda^0$ ,  $\mathbf{g}$  is in the  $\delta_{\mathbf{g}, \epsilon}$ -sup-norm neighborhood of  $\mathbf{g}^0$  and  $\Sigma$  is in the  $\delta_{\Sigma, \epsilon}$ -sup-norm neighborhood of  $\Sigma^0$  then  $KL(f_{\Lambda, \mathbf{g}, \Sigma}, f^0) < \epsilon$ . Therefore  $\Pi_f[KL_\epsilon(f^0)] > 0$ .  $\square$

### Proof of Proposition 3

Let  $U_\epsilon(f^0) := \{f : \int |f - f^0| d\mathbf{x} < \epsilon\}$ . Our proof uses Theorem 2 of Ghosal et al. (1999), which provides sufficient conditions under which the posterior probability assigned to strong neighborhoods of the true data-generating density converge to one almost surely. Their result involves conditions on the size of the parameter space in terms of  $L_1$  metric entropy. Before proceeding, we review  $L_1$  metric entropy and Theorem 2 of Ghosal et al. (1999).

**Lemma 1.** *[Theorem 2 in Ghosal et al. (1999)] Let  $\Pi$  be a prior on  $\mathcal{F}$ . Suppose  $f_0 \in \mathcal{F}$  is in the Kullback-Leibler support of  $\Pi$  and let  $U = \{f : \int |f - f_0| dy < \epsilon\}$ . If there is a  $\delta < \epsilon/4$ ,  $c_1, c_2 > 0, \beta < \epsilon^2/8$  and  $\mathcal{F}_n \subset \mathcal{F}$  such that for all large  $n$  :*

- (1)  $\Pi(\mathcal{F}_n^c) < c_1 \exp(-nc_2)$ , and,
- (2) The  $L_1$  metric entropy,  $J(\delta, \mathcal{F}_n) < n\beta$ , then  $\Pi(U | Y_1, Y_2, \dots, Y_n) \rightarrow 1$  a.s.  $P_{f_0}$ .

The  $L_1$  metric entropy  $J(\delta, \mathcal{G})$  for  $\mathcal{G} \subset \mathcal{F}$  is defined as the minimum of

$$\log \left( k : \mathcal{G} \subset \bigcup_{i=1}^k \left\{ f : \int |f - f_i| dy < \delta, f_1, f_2, \dots, f_k \in \mathcal{F} \right\} \right).$$

*Proof.* We verify that our proposed prior framework satisfies the two conditions. Let  $\mathcal{H}_n$  denote a subset of the parameter space and adopt the decomposition such that  $\mathcal{H}_n = \mathcal{H}_{1n} \otimes \mathcal{H}_{2n}$ , where  $\mathcal{H}_{1n} = \{(\mathbf{\Lambda}, \mathbf{g}) : \|\mathbf{\Lambda}\mathbf{g}\|_\infty \leq M_n\}$  and  $\mathcal{H}_{2n} = [L_n, \infty)^p$  where  $M_n = O(\sqrt{n})$  and  $L_n \rightarrow 0$ .

Since the prior for each element of  $\mathbf{\Lambda}$  and each spline slope characterizing  $\mathbf{g}$  is Gaussian, we obtain  $\Pi(\mathcal{H}_{1n}^c) \leq A_1 \exp(-B_1 M_n^2)$ . For  $\mathcal{H}_{2n}$ , we can choose  $L_n$  small enough such that  $\nu(0, L_n) \leq A_2 \exp(-B_2 n)$ , where  $\nu$  is the inverse-Gamma prior.

By Theorem 2.7.1 in Wellner et al. (2013), if  $\mathcal{X}$  is a bounded, convex subset of  $\mathbb{R}^d$  with nonempty interior, and  $m$  is a 1-Lipschitz mapping from  $\mathcal{X}$  to  $\mathbb{R}$ , then there exists a constant  $C_1$  such that the  $L_\infty$  entropy of  $m(\mathcal{X}) \leq C_1 \lambda(\mathcal{X}^1) \delta^{-d}$  for every  $\delta > 0$ , where  $\lambda(\mathcal{X}^1)$  is the Lebesgue measure of the set  $\{x : \|x - \mathcal{X}\| < 1\}$ . In the NIFTY setting,  $\mathcal{X}$  is a  $K$ -dimensional unit cube. Since  $\mathbf{g}$  is modeled by linear splines,  $(\mathbf{\Lambda}\mathbf{g})_j$  is 1-Lipschitz for any  $j = 1, \dots, p$ . Therefore, we have bounded the  $L_1$  metric entropy as  $J(\delta, \mathcal{H}_{1n}) < C_1 M_n / (3\delta^K)$ .

This implies there are  $C^* = \lceil \exp(C_1 M_n / (3\delta^K)) \rceil$  elements  $\boldsymbol{\mu}_1, \boldsymbol{\mu}_2, \dots, \boldsymbol{\mu}_{C^*}$  such that

$$\mathcal{H}_{1n} \subset \bigcup_{i=1}^{C^*} \left\{ (\mathbf{\Lambda}, \mathbf{g}) : \max_j \int_0^1 |[\mathbf{\Lambda}\mathbf{g}(\mathbf{u})]_j - [\boldsymbol{\mu}_i(\mathbf{u})]_j| d\mathbf{u} < \delta \right\}.$$

We now consider the sieve

$$\mathcal{F}_n = \{f_{(\mathbf{\Lambda}, \mathbf{g}, \boldsymbol{\Sigma})} : (\mathbf{\Lambda}, \mathbf{g}) \in \mathcal{H}_{1n}, \text{diag}(\boldsymbol{\Sigma}) \in \mathcal{H}_{2n}\}.$$

Clearly  $\mathcal{F}_n \subseteq F$  and  $\mathcal{F}_n \uparrow F$ . Observing that  $\mathcal{H}_n \subset \mathcal{F}_n$  implies  $\Pi(\mathcal{F}_n^c) = (\Pi^* \otimes \nu)(\mathcal{H}_n^c) = (\Pi^* \otimes \nu) \{(\mathcal{H}_{1n}^c \otimes \mathcal{H}_{2n}) \cup (\mathcal{H}_{1n} \otimes \mathcal{H}_{2n}^c)\} \leq c_1 \exp(-c_2 n)$ ,  $c_1, c_2 > 0$ . This proves the first condition in Lemma 1.

We now show that  $J(\delta, \mathcal{F}_n)$  can be controlled by  $J(\delta, \mathcal{H}_n)$  times a constant. Given a fixed value of  $\mathbf{u}$  in the  $K$  unit cube, for simplicity of notation, we denote the  $j$ th entry in  $\boldsymbol{\mu}_i(\mathbf{u})$  as  $\mu_{ij}$  and denote the  $j$ th entry in  $\boldsymbol{\Lambda}\mathbf{g}(\mathbf{u})$  as  $\hat{\mu}_j$ . It can be shown for  $L_n$  small enough, if  $\mu_{ij} < \hat{\mu}_j$ , then

$$\begin{aligned} & \int |\phi_\sigma(y - \hat{\mu}_j) - \phi_{L_n}(y - \mu_{ij})| dy \\ &= (2\pi\sigma^2)^{-1/2} \int_{G_y} \exp\left\{-\frac{(y - \hat{\mu}_j)^2}{2\sigma^2}\right\} - (2\pi L_n^2)^{-1/2} \int_{G_y} \exp\left\{-\frac{(y - \mu_{ij})^2}{2L_n^2}\right\} \\ &+ (2\pi L_n^2)^{-1/2} \int_{G_y^c} \exp\left\{-\frac{(y - \mu_{ij})^2}{2L_n^2}\right\} - (2\pi\sigma^2)^{-1/2} \int_{G_y^c} \exp\left\{-\frac{(y - \hat{\mu}_j)^2}{2\sigma^2}\right\} \\ &\leq 2(\hat{\mu}_j - \mu_{ij}) / (2\pi\sigma^2)^{1/2} + 2(\hat{\mu}_j - \mu_{ij}) / (2\pi L_n^2)^{1/2} \leq 4(\hat{\mu}_j - \mu_{ij}) / (2\pi L_n^2)^{1/2}, \end{aligned}$$

where  $G_y = \{y \in \mathbb{R} : y > (\mu_{ij} + \hat{\mu}_j)/2\}$ . Similarly, we have  $\int |\phi_\sigma(y - \hat{\mu}_j) - \phi_{L_n}(y - \mu_{ij})| dy \leq 4(\hat{\mu}_j - \mu_{ij}) / (2\pi L_n^2)^{1/2}$  when  $\mu_{ij} \geq \hat{\mu}_j$ . This implies that the sequence  $f_j := f_{\boldsymbol{\mu}_j, \boldsymbol{\Sigma}}$  is a  $\delta$ -cover of  $\mathcal{F}_n$  when  $\boldsymbol{\mu}_j$  is a  $\delta$ -cover of  $\mathcal{H}_{1n}$ , because whenever  $\max_j \int_0^1 |\mu_{ij} - \hat{\mu}_j| du < \delta$ ,

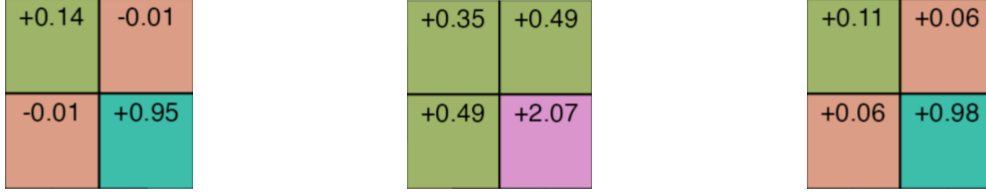
$$\int |f_{\boldsymbol{\mu}_i} - f_{\boldsymbol{\Lambda}, \mathbf{g}, \boldsymbol{\Sigma}}| d\mathbf{y} \leq \prod_{j=1}^p (4(\hat{\mu}_j - \mu_{ij}) / (2\pi L_n^2)^{1/2}) \leq C_2(\delta/L_n)^p.$$

This suggests that  $J(\delta, \mathcal{F}_n) \leq C_3 M_n (L_n/\delta)^{pK}$ . Since  $M_n = O(\sqrt{n})$ , we can set  $\delta < \epsilon/4$  and choose  $\beta < \epsilon^2/8$  such that  $J(\delta, \mathcal{F}_n) < n\beta$ , and the second condition in Lemma 1 is satisfied.  $\square$

# Supplemental Materials

## A Consequences of posterior distributional shift

We demonstrate in this continuation of Example 1 that latent factor distributional shift leads to bias in posterior estimators of the covariance matrix. Recall that the two marginal distributions in Example 1 are  $x_{i1} \sim \text{Beta}(0.4, 0.4)$  and  $x_{i2} \sim \text{Gamma}(1, 1)$ . The empirical covariance of  $\mathbf{x}_i$ , the covariance estimator  $\hat{\mathbf{\Lambda}}\hat{\mathbf{\Lambda}}^T + \hat{\mathbf{\Sigma}}$  (usually applied in linear factor models) and a factor model-based bias-corrected covariance estimator  $\hat{\mathbf{\Lambda}}\text{cov}(\hat{\boldsymbol{\eta}}_i, i = 1, \dots, N)\hat{\mathbf{\Lambda}}^T + \hat{\mathbf{\Sigma}}$  are displayed in Figure S1, where  $\hat{\mathbf{\Lambda}}$  and  $\hat{\mathbf{\Sigma}}$  are posterior means after post-processing via MatchAlign algorithm Poworoznek et al. (2021).



(a) Empirical covariance of  $\mathbf{x}_i$  in the data. (b) Posterior estimation via  $\hat{\mathbf{\Lambda}}\hat{\mathbf{\Lambda}}^T + \hat{\mathbf{\Sigma}}$ . (c) Posterior estimation via  $\hat{\mathbf{\Lambda}}\text{cov}(\hat{\boldsymbol{\eta}}_i, i = 1, \dots, N)\hat{\mathbf{\Lambda}}^T + \hat{\mathbf{\Sigma}}$ .

Figure S1: Fitting a Gaussian linear factor model on a non-Gaussian dataset, the usually applied covariance estimator (panel b) leads to significant bias. Good performance of the estimator in (c) demonstrates that the posterior of  $\mathbf{\Lambda}$  compensates for posterior drift in the covariance of the latent factors.

## B Computational Details

### Prior specification

We first introduce some notation to formulate the nonlinear mappings. We divide the  $[0, 1]$  interval evenly into  $L$  pieces. Let  $0 = s_0, s_1, \dots, s_{L-1}, s_L = 1$  denote the endpoints of each piece and  $\alpha_{lh}$  denote the slope for the  $l$ -th piece. Then we have a linear representation of  $g_h$  as

$$g_h(u) = \alpha_{0h} + \alpha_{1h}(u - s_0)1\{u \in [s_0, s_1)\} + \dots + \alpha_{Lh}(u - s_{L-1})1\{u \in [s_{L-1}, s_L)\}.$$

Through simplifying  $\mathbf{g}$  to consist of monotone piecewise linear functions, we reduce inference of the nonlinear mappings to a simpler problem of estimating the slope parameters  $\{\alpha_{lh}\}_{l,h}$ .

As the number of latent factors is typically unknown in practice, we would ideally allow for uncertainty in choosing this number. In simpler linear factor model settings, it has become popular to rely on over-fitted factor models that choose an initial upper bound on the number of factors, and then rely on shrinkage priors on the loadings to favor effective deletion of extra factors that are unneeded. Due to the structure of the NIFTY model, it is straightforward to directly adapt shrinkage strategies used in Gaussian linear factor models (Refer to Section 2 for a discussion of this literature).

Considering the above discussion and that of Section 2.3, we assign the following priors:

$$\begin{aligned}
\lambda_{jh} &\sim N(0, \tau\gamma_{jh}\sigma_j^2), \\
\gamma_{jh} &\sim \mathcal{C}^+(0, 1), \\
\tau &\sim \mathcal{C}^+(0, 1), \\
\alpha_{lh} &\sim N^+(0, \sigma_a^2), \\
\sigma_1^2, \dots, \sigma_P^2 &\sim \text{Inv-Gamma}(a_\sigma, b_\sigma), \\
\Pi_{\mathbf{u}_k}(u_{ik}) &= \prod_i 1(u_{ik} \in [0, 1]) \exp(-\nu \mathcal{W}^2(U_k, U))
\end{aligned} \tag{S1}$$

where  $N^+$  denotes the half-normal distribution and  $\text{Inv-Gamma}(a_\sigma, b_\sigma)$  denotes an inverse-Gamma distribution with shape parameter  $a_\sigma$  and rate parameter  $b_\sigma$ .

## MALA-within-Gibbs posterior sampling

In this section, we describe an algorithm to obtain posterior samples. We divide the parameters  $(\mathbf{\Lambda}, \alpha_{lh}, u_{ik}, \sigma_j^2)$  into five blocks, and sample each block of parameters from their joint distribution conditioned on all other blocks. Conjugate updates are available for  $\mathbf{\Lambda}$ ,  $\alpha_{lh}$  and  $\sigma_j^2$ , but not for  $u_{ik}$ , due to the constraint relaxation term in the prior specification. Hence, we use a Metropolis-

adjusted Langevin algorithm (MALA) (Roberts and Tweedie, 1996; Roberts and Stramer, 2002)

to update the  $u_{ik}$ 's.

The following steps describe the MALA-within-Gibbs sampling procedure.

Parameters:  $\mathbf{\Lambda}(\lambda_{jh}), \alpha_{lh}, u_{ik}, \sigma_j^2, \quad j = 1, \dots, P, \quad h = 1, \dots, H, \quad k = 1, \dots, K, \quad i = 1, \dots, N.$

Step 1: The rows of  $\mathbf{\Lambda}$  has conditionally independent conjugate Gaussian distributions. Update the  $j$ -th row ( $j = 1, \dots, P$ ) of  $\mathbf{\Lambda}$  via

$$\mathbf{\Lambda}_j | - \sim N_H(\mathbf{V}_j \sum_{i=1}^n \boldsymbol{\eta}_i x_{ij} \sigma_j^{-2}, \mathbf{V}_j)$$

where  $\mathbf{V}_j = \text{diag}[(\tau\gamma_{j1})^{-1}, \dots, (\tau\gamma_{jH})^{-1}] + \sigma_j^{-2} \boldsymbol{\eta} \boldsymbol{\eta}^T.$

Step 2: update  $\sigma_1^2, \dots, \sigma_P^2,$  via conditionally independent inverse-Gamma distributions,

$$\sigma_j^{-2} | - \sim \text{Gamma}(a_\sigma + N/2, b_\sigma + \frac{1}{2} \sum_{i=1}^n (x_{ij} - \mathbf{\Lambda}_j^T \boldsymbol{\eta}_i)^2).$$

Step 3: let  $\boldsymbol{\alpha}$  denote the vector containing all  $\alpha_{lh}.$  Moreover, let  $u_{ikl}$  denote  $\min[\max(u_{ik} - s_{l-1}, 0), s_l - s_{l-1}].$  Then the posterior of  $\boldsymbol{\alpha}$  is a conjugate Gaussian distribution conditioned on other parameters:

$$\begin{aligned} \boldsymbol{\alpha} &\sim N_{LH}(\mathbf{m}^\alpha, \boldsymbol{\Sigma}^\alpha), \\ \mathbf{m}^\alpha &= \boldsymbol{\Sigma}^\alpha \boldsymbol{\mu}^\alpha, \quad \mu_{lh}^\alpha = \sum_{i=1}^N \sum_{j=1}^P (x_{ij} - \mathbf{\Lambda}_j \boldsymbol{\eta}_i + \lambda_{jh} \alpha_{lh} u_{ikhl}) / \sigma_j^2, \\ \boldsymbol{\Sigma}_{lh, l'h'}^\alpha &= \text{Cov}(\alpha_{lh}, \alpha_{l'h'}) = \sum_{i=1}^N \sum_{j=1}^P \lambda_{jh} \lambda_{j'h'} u_{ikhl} u_{i'k'h'l'} / \sigma_j^2. \end{aligned}$$

Step 4: update  $u_{ik}$ 's using the Metropolis-adjusted Langevin algorithm (MALA). Let  $\pi(u | -)$

denote the conditional posterior density. At step  $t,$  propose  $\tilde{u}^{t+1}$  using the Langevin diffusion

$$\tilde{\mathbf{u}}^{t+1} = \mathbf{u}^t + \epsilon \nabla \log \pi(\mathbf{u}^t | -) + \sqrt{2\epsilon} \mathbf{v},$$

where  $\epsilon > 0$  is a small step-size and each entry in  $\mathbf{v}$  is generated independently from a standard normal distribution. This proposal is accepted with probability

$$p_{\text{accept}} = \min \left\{ 1, \frac{\pi(\tilde{\mathbf{u}}^{t+1})q(\mathbf{u}^t | \tilde{\mathbf{u}}^{t+1})}{\pi(\mathbf{u}^t)q(\tilde{\mathbf{u}}^{t+1} | \mathbf{u}^t)} \right\},$$

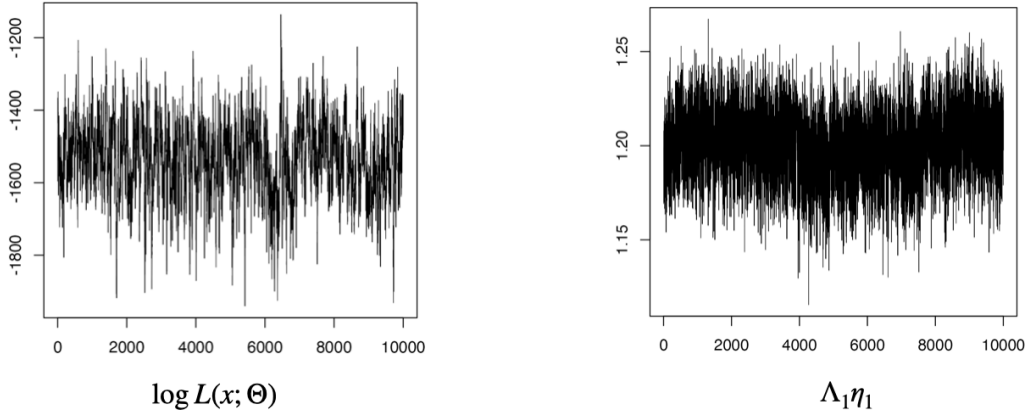
where  $q(\mathbf{u}' | \mathbf{u}) \propto \exp\left(-\frac{1}{4\epsilon}\|\mathbf{u}' - \mathbf{u} - \epsilon\nabla \log \pi(\mathbf{u})\|_2^2\right)$  and

$$\log \pi(\mathbf{u}^t | -) = -\sum_{i=1}^N \sum_{j=1}^P [x_{ij} - \sum_{h=1}^H \lambda_{jh} \sum_{l=1}^L \alpha_{lh} u_{ik_h l}]^2 / \sigma_j^2 - \nu \sum_{i=1}^N \|u_{(i)k} - u_{(i)}^0\|_2^2.$$

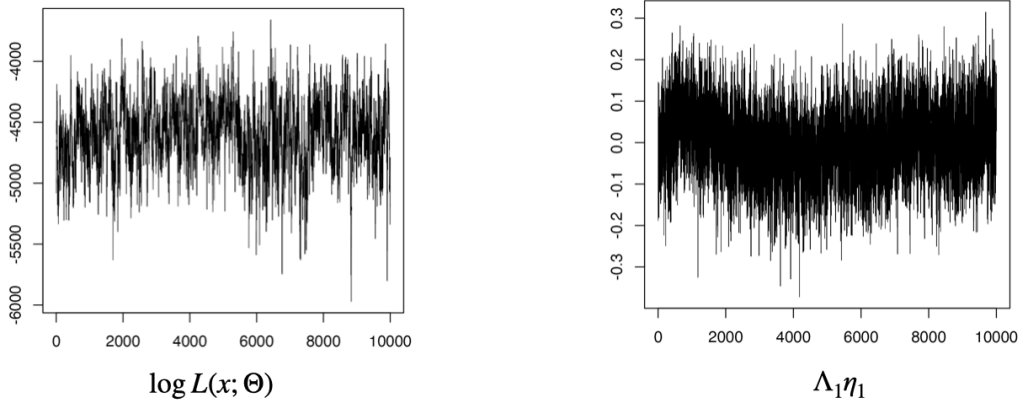
Step 6: update the hyperparameters  $(\tau^2, \rho_{hk}^2, \phi_{jh}, \theta_h)$  according to Makalic and Schmidt (2015) and Legramanti et al. (2020).

## B.1 MCMC diagnostics

For each simulated experiment in section 5.1, we now show additional results about the computation efficiency of Markov Chain Monte Carlo. Figure S2 displays trace plots and autocorrelation functions of 10000 samples (after discarding a burn-in of 10000) for  $\mathbf{\Lambda}_1 \boldsymbol{\eta}_1$ .



(a) Trace plots of curved shape data in  $\mathbb{R}^{10}$ .



(b) Trace plots of the common chiffchaff bird calls data.

Figure S2: Trace plots on log-likelihood (left column) and  $\Lambda_1 \eta_1$  (right column) in the simulated two-curve experiment (panel a) and the bird data augmentation for common chiffchaff (panel b).

## C Simulation Results

### C.1 Simulation setup for each method

All of the numerical experiments are run on an Intel(R) Xeon(R) CPU E5-2680 v3 with 2.50GHz processor. We list the version we used for each algorithm, and choices of tuning parameters or initializations for each method as follows.

**Setup for NIFTY:** We choose  $\nu$  based on results from a preliminary sensitivity analysis; refer to S 3.2 below. We choose the remaining hyper-parameters in the prior specification to be  $\sigma_a^2 = 1$ ,  $a_\sigma = 100$ ,  $b_\sigma = 1$ .

**Setup for PPCA:** We use R package `cusp` (Legramanti et al., 2020) to run the Gaussian linear



factor models. The hyper-parameter specification of CUSP is  $a_\sigma = 100, b_\sigma = 1, a_\theta = 2, b_\theta = 2, \theta_\infty = 0.01$ . We fix the latent dimension to be five.

For the above two Bayesian methods, we run the Markov chain for 10,000 iterations and discard the first 5,000 samples as a burn-in.

**Setup for VAE:** Through a preliminary study of the literature, we find the recently introduced sparseVAE (Moran et al., 2022) performs better than the original VAE and  $\beta$ -VAE in terms of factor interpretability. Therefore, we use the GitHub repository from the sparseVAE paper in our VAE implementations. Our tuning parameter and network parameters are similar to the setting in the numerical experiments in Moran et al. (2022). The latent space dimension is fixed to be five in all the experiments. When training the neural network, we use three hidden layers, set each layer dimension to 100, and use a batch of size 100 in each iteration. During 500 epochs of training, the learning rate is fixed to be 0.01.

**Setup for GP-LVM:** We used the python repository `pyro` to implement GP-LVMs (Titsias and Lawrence, 2010). The number of latent dimensions is pre-specified to be 5, and the number of inducing variables is set to 50. Similar to the training of VAE, there are 500 epochs and the batch size in each epoch is 100. The learning rate is fixed to be 0.01. Following instructions in the GP-LVM documentation, factors are initialized with PCA.

In all of the above methods, we initialize  $\sigma_j$  with a small value, to allow fast convergence to the posterior mode. Specifically, for NIFTY, we fix  $\Sigma$  for the first 1000 iterations during the burn-in stage.

## C.2 Sensitivity analysis on $\nu$

We conduct a numerical study of the sensitivity of NIFTY to the choice of hyperparameter  $\nu$ . As a quick recap, this parameter regulates the “distributional distance” between the latent locations and a uniform distribution. We let  $\nu$  vary from  $\{0, 1, 10^2, 10^3, 10^4\}$  in the simulated example S1 with initial sample size 200. Figure S3 panel (a) shows a choice of  $\nu = 10^3$  achieves the smallest

Wasserstein distance and largest effective sample size, and hence is considered the best choice in this example. When  $\nu = 0$  or is very small, no constraint or a very loose constraint is placed on the latent locations  $\mathbf{u}$ . Panels (b)-(c) indicate that the chains converge near the mode quickly but mix slowly, and the large out-of-sample Wasserstein distance shows clear evidence of posterior drift in the latent variable distribution away from uniform. As  $\nu$  increases to 100 or the even better value of 1000 we see much less distributional shift and improved mixing. Values in this range are recommended. If we increase  $\nu$  too much, the constraint becomes too strong and performance starts to degrade. Therefore, we suggest running a preliminary study to choose an appropriate  $\nu$  that balances the distributional control over the uniform latent locations and the posterior information inferred from the data.

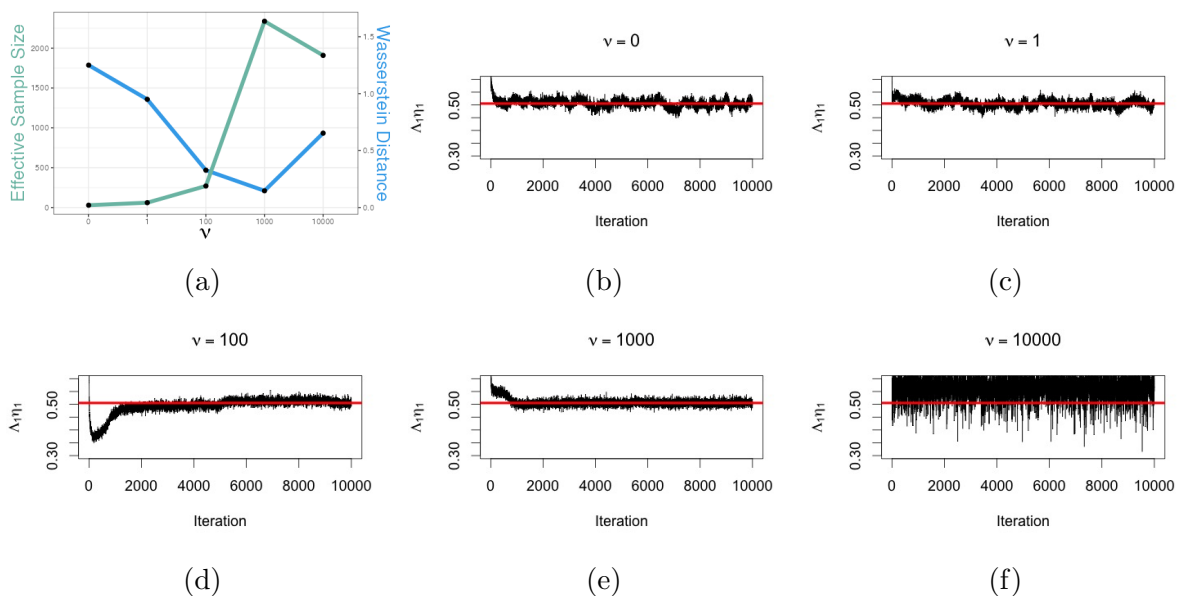


Figure S3: Effect of different choices of  $\nu$  on density estimation and sampling efficiency. Panel (a): Effective sample size (left axis, green line) and Wasserstein distance between generated data and true distribution (right axis, blue line) for different values of  $\nu$ . Panel (b)-(f): Trace plots of  $\Lambda_j \eta_i$  for different values of  $\nu$ .